MASTERARBEIT

Titel der Masterarbeit

„Ageing of neural stem cells in a

Parkinson's disease Model "

Verfasserin

Ingeborg Menzl, B. rer. nat.

angestrebter akademischer Grad

Master of Science (MSc)

Wien, 2013

Abstract

Parkinson's disease occurs through loss of neurons during ageing and is one of the common neurodegenerative diseases next to Alzheimer's disease. It affects 4 % of the elderly population and is characterized by motor-dysfunctional symptoms as well as non-motor symptoms. Mutations in the LRRK2 protein seem to trigger the process of neurodegeneration, especially apoptosis of dopaminergic neurons. Furthermore, LRRK2 was detected to influence the miRNA pathway in favor to maintain proliferation of neural stem cells. Therefore, we focused on one specific mutation (G2019S) in the kinase domain of the protein which is spread in familial as well as sporadic Parkinson's disease. The neuroepithelial stem cells bearing the LRRK2 mutation G2019S, displayed a 3-fold higher apoptosis rate in comparison to WT cells during proliferation as well as differentiation. Additionally, autophagy seemed to be diminished in both states. These results confirm the neural toxicity of the LRRK2 G2019S mutation already at the neuroepithelial stem cell stage and its increase during ageing. In addition, an interaction between LRRK2 and the neuronal differentiation inducing protein TRIM32 was observed. Both proteins have been exhibited to be involved in the miRNA pathway. We were able to detect the miRNAs let-7a and miR-184 as well as the mRNAs *e2f1* and *dp1* in LRRK2-TRIM32 complexes. Different expression levels of LRRK2 and TRIM32 during development and ageing, further verified their importance in neurogenesis.

Abstract

Zusammenfassung

Die Parkinson-Krankheit zählt zu den neurodegenerativen Erkrankungen. Eines der wichtigsten Charakteristika ist der Verlust von dopaminergen Neuronen in der Substantia nigra. Dies manifestiert sich in Muskelzittern sowie –erstarren, verlangsamten Bewegungen und Haltungsinstabilität, zusätzlich treten auch kognitive und psychische Störungen auf. In letzter Zeit wurden Mutationen in Genen entdeckt, die eine wichtige Rolle in der Ausbildung der familiären Form von Parkinson spielen. LRRK2 ist eines dieser Proteine, es interagiert mit dem mikro-RNA System und beeinflusst es zugunsten von Proliferation wodurch die Differenzierung der Stammzellen inhibiert wird. Mutationen in LRRK2 bewirken eine Beschleunigung des neurodegenerativen Prozesses, präferenziell das Absterben von Dopamin produzierenden Neuronen. In dieser Studie wurde der Effekt der Mutation G2019S in LRRK2 auf Neuroepithelzellen untersucht, die sowohl in familiären- als auch sporadischen Parkinson Patienten nachgewiesen werden konnte. Neuroepithelzellen welche die LRRK2-G2019S Mutation tragen, zeigten im Vergleich zu Wildtypzellen einen 3-fach höheren Anteil apoptotischer Zellen und eine Reduzierung im Recycling von dysfunktionalen Mitochondrien unter proliferierenden und differenzierenden Bedingungen. Diese Resultate bestätigen den neurotoxischen Effekt der G2019S Mutation und weisen diesen bereits in Neuroepithelzellen nach. Es war ebenfalls möglich eine Interaktion zwischen LRRK2 und dem Protein TRIM32, welches wichtig für die Induktion der neuronalen Differenzierung ist, nachzuweisen. Dies ist von besonderer Bedeutung da beide Proteine mit mikro-RNAs interagieren aber gegensätzliche Auswirkungen haben. Im LRRK2-TRIM32 Komplex wurden zusätzlich die mikro-RNAs let-7a und miR-184 sowie die mRNAs für *e2f1* und *dp1*

nachgewiesen. Eine Fluktuation in den Expressionslevels von LRRK2 und TRIM32 während der Embryonalentwicklung und während des Alterungsprozesses verdeutlichen deren Bedeutung und Einfluss.

1 Introduction

1.1 Parkinson's disease

Parkinson's disease (PD) is the second most common neurodegenerative disorder after Alzheimer's disease in the "over 50" population and was first described by James Parkinson in 1817. PD is characterized by progressing motor symptoms like bradykinesia, resting tremor or rigidity but also non-motor functions are negatively affected. Responsible for these motor symptoms, is the progressive loss of dopaminergic neurons in the substantia nigra pars compacta and the consequent reduction of dopamine in the nigrostriatal projections. However, the progression of PD is supposed to start in the brainstem nuclei and the olfactory bulb extending to the midbrain, the mesocortical and lastly the cortical regions (Braak et al., 2003).

To date, it is thought that environmental as well as genetic factors are the two main causes of PD. In most cases, the disease occurs sporadic, but there were several genes discovered during the last decade that, when mutated, can cause familial forms of PD. The progression of PD can be categorized into six neuropathological stages and it takes between five to seven years before the symptoms become manifested (reviewed in Braak et al., 2004). However, the crucial mechanisms for the aetiology of PD are not fully understood.

One reason for the death of neurons may be the accumulation of Lewy bodies. These are intracellular neuronal aggregates containing misfolded proteins, especially α-Synuclein (Kahle et al., 2000). Mutations in the gene for *α-synuclein* circumvent its degradation and lead to elevated expression levels (Cuervo et al., 2004). Therefore, the mutated forms accumulate in Lewy bodies which not necessarily lead to cell

death but the disruption of neuronal plasticity (Nuber et al., 2008). In addition, mutations in genes for ubiquitin carboxylase L1, PINK1, DJ1 and Parkin have been found to play a role in PD (Abou-Sleiman et al., 2004; Choi et al., 2004; Ferraris et al., 2009; Shimura et al., 2001). These proteins are expressed all over the brain and have different impacts on the disease. The majority of these protein mutations were found in familial forms of PD.

Moreover, mutations in the gene for LRRK2 were primarily identified in cases of familial forms of PD all over the world. Interestingly, only mutations that affect the enzymatic function of LRRK2 have been shown in familial PD. Although these mutations are inherited dominantly, it is an incomplete mutation; therefore, not all carriers of the mutated LRRK2 develop PD in their lifetime. Nevertheless, the LRRK2 mutations were detected as well in sporadic PD (reviewed in Cookson, 2010). Furthermore, biochemical changes have been identified in the PD brains, for example increased oxidative stress and damage, mitochondrial dysfunction and inflammation (Schapira, 1999).

1.2 Adult neurogenesis

The mammalian nervous system originates from neural stem cells (NSCs). Stem cells in general are described to self-renew and to give rise to various types of differentiated cells (Gage, 1998). Therefore, the stem cell can either undergo symmetric divisions that result in two identical stem cells or asymmetric divisions which generate one stem cell and a more differentiated progeny (reviewed in Doe, 2008).

Adult neurogenesis describes the generation of new neurons by dividing stem cells in the adult brain. Active neurogenesis and neural stem cells in the adult brain are only present in two neurogenic regions, the subgranular zone (SGZ) of the dentate gyrus in the hippocampus and the subventricular zone (SVZ) of the lateral ventricles in the forebrain. In both regions, newborn neurons are produced, for example the SVZ gives rise to progenitors which migrate along the rostral migratory stream (RMS) to the olfactory bulb, where they differentiate into interneurons (Lois and Alvarez-Buylla, 1994).

Adult neurogenesis is a dynamic process that is influenced by several physiological and pathological factors. (reviewed in Ming and Song, 2005; Duan et al., 2008; Zhao et al., 2008). Furthermore, adult neurogenesis plays an important role in learning and memory. An increase of NSC activity is suggested to repair brain damage and counteract neural loss but the factors which alter the levels of neurogenesis during ageing have not been elucidated. Importantly, during ageing, the number of NSCs is stabile but proliferation is deteriorating and more cells are in a quiescent state (Hattiangady and Shetty, 2008; Lugert et al., 2010) In contrast, a recent study showed a decline of hippocampal NSCs during ageing caused by their

conversion into mature hippocampal astrocytes. These results are a possible explanation for the decline of adult neurogenesis and an increase of astrocytes in the adult brain. However, they did not exclude a remaining pool of NSC but proposed a "disposable stem cell model" in the adult brain (Encinas et al., 2011)

One key player in this dynamically regulated process is dopamine. Dopamine controls the activity of NSCs already during development of the mammalian brain. The depletion of this neurotransmitter during the development of PD leads to a reduced proliferation of NSCs as well as to decreased neurogenesis in adult brains. The close proximity of dopaminergic fibers to cells of the subependymal zone is thought to facilitate the influence of dopamine on NSCs in the adult brain (Höglinger et al., 2004). Therefore, the absence of dopamine, which is a hallmark of Parkinson's disease, is associated with neurodegeneration. On the contrary, results from another study exhibited neither a decrease of proliferation activity nor an effect of dopamine on stem cell proliferation (Van den Berge et al., 2011).

However, 5 to 10 years before a manifestation of motor symptoms, already half of the cells in the substantia nigra were lost. Symptoms like hyposmia, depression and anxiety are caused by defects in adult neurogenesis. Furthermore, a decrease in number of proliferating cells was examined in the SVZ of PD patients. Mouse models carrying a α-synuclein mutation exhibited an age-dependent reduction in proliferation an reduced survival of new neurons (Winner et al., 2008). Moreover, transgenic LRRK2 models indicated changed dopamine levels as well as reduction in proliferation and survival (Winner et al., 2011). Despite the absence of a "perfect" PD animal model, an impairment of adult neurogenesis resulting in diminishing proliferative activity and low survival rate of new born neurons is consistent.

1.3 Leucine-repeat rich kinase 2 (LRRK2)

Leucine-repeat rich kinase 2 (LRRK2) was the first protein which has been discovered in relation to the nigrostriatal dopamine system, especially in the target areas of dopamine (Galter et al., 2006). Additionally, LRRK2 was detected in the neurogenic niches of the adult brain. Moreover, mutations of this protein can lead to familial and sporadic PD.

LRRK2 is a 280 kDa protein that contains a variety of functional domains, for instance a kinase and GTPase domain. Besides these two enzymatic domains, LRRK2 contains various protein-protein interaction domains like the leucine-rich repeat, WD40 and an Ankyrin repeat. The WD40 domain, in close proximity to the C-terminus, enables the formation of functional dimers by self-association of LRRK2 to autoregulate its enzymatic activity (Jorgensen et al., 2009). LRRK2 has been implicated in the regulation of cell survival and cell death pathways. Moreover, it has been described to interact with the cytoskeleton and trafficking proteins and thus influence vesicle movement and membrane fusion (Shin et al., 2008).

To date, around 30 different LRRK2 mutations have been discovered. Some of the LRRK2 mutations cause autosomal dominant PD with an increased penetrance with age. The mutation G2019S, for instance, was found in many families all over the world, it is inherited dominantly with late onset but incomplete penetrance. Interestingly, the G2019S mutation has been found in sporadic PD cases as well; the generation to generation transmission is still not well understood. (reviewed in Greggio and Cookson, 2009; Halliday and McCann, 2010). LRRK2 mutations affect different pathways and can result in abnormal protein phosphorylation, reduction of neurite length and branching, impaired vesicle endocytosis and increased apoptosis

in primary neurons (Lu and Tan, 2008) (reviewed in Santpere and Ferrer, 2009). However, the pathology of the LRRK2 mutations is highly diverse which confirms the importance of LRRK2 in multiple cellular processes of neurons. LRRK2 is further proposed to function upstream of other genes which are linked to PD (reviewed in Mata et al., 2006)

1.4 Micro-RNA regulation

Micro-RNAs (miRNAs) are small noncoding RNAs that regulate gene expression via post-transcriptional inhibition or degradation of complementary mRNAs. To fulfill their functions, microRNAs bind to Argonaute proteins and assemble into the RNA-induced silencing complex (RISC). To inhibit the expression of the target mRNA, the RISC binds target sites in the 3' untranslated region (UTR) of the mRNA. Is the binding between target mRNA and miRNA incomplete the silencing is achieved by preventing translation. Whereas Ago cleaves the mRNA through complete binding of the target sequence and subsequently leads to mRNA degradation (Bartel, 2004).

During adult neurogenesis, miRNAs are important for fine tuning of gene expression. Several miRNAs have been discovered to induce and support neuronal differentiation of NSCs. For instance, the miRNA let-7 is proposed to regulate cell homeostasis in the adult tissue and to repress cell cycle progression (Johnson et al., 2007). Furthermore, let-7a induces neuronal differentiation via degradation of c-Myc (Rybak et al., 2008; Wulczyn et al., 2007). However, other miRNAs counteract differentiation and promote proliferation.

MiRNAs have been found in reduced levels in PD brains (reviewed in Mouradian, 2012). Moreover, LRRK2 was discovered to negatively regulate the

miRNA pathway. An increase of LRRK2 kinase activity, for example by the G2019S mutation, leads to circumvention of the translational repression of *e2f1* and *dp1* mRNAs which results in death of dopaminergic neurons. LRRK2 is important for the stability of dAgo1 and therefore, enables the miRNAs let-7a and miR-184[*] to regulate the mRNA translation (Gehrke et al., 2010).

1.5 Tripartite motif protein 32 (TRIM32)

The tripartite motif protein 32 (TRIM32) belongs to the TRIM-NHL family which is characterized by a RING domain, one or two B-boxes, a coiled-coil domain and a C-terminal NHL domain (Reymond et al., 2001). TRIM proteins containing a RING finger domain are E3 ubiquitin ligases which mediate the transfer of ubiquitin from the E2 conjugating enzyme to a specific target protein. Although the function of the B-boxes has not been clarified so far, it has been suggested that they influence the E3 enzyme activity (Han et al., 2011). Some TRIM proteins are found in specific subcellular compartments so called "cytoplasmic bodies" and can interact with each other via the coiled-coil domains (Reymond et al., 2001). Members of this family are associated with transcriptional regulation, development, cell growth, apoptosis and oncogenesis. Mutations of TRIM32 have been implicated in various diseases, like the Bardet-Biedl syndrome or Limb-Girdle muscular dystrophy type 2H (Chiang et al., 2006; Frosk et al., 2002).

Previous studies have identified substrates of TRIM32 like actin and dysbindin (Kudryashova et al., 2009; Locke et al., 2009). Furthermore, TRIM32 has been detected to induce neuronal differentiation via stabilization of the retinoic acid receptor α in neuroblastoma cells (Sato et al., 2011). Another work revealed the

interaction of TRIM32 and the protein kinase C ζ during stem cell maintenance, this interaction prevents the translocation of TRIM32, which is essential for the induction of neuronal fate (Hillje et al., 2011). It has also been reported that TRIM32 is involved in differentiation of muscle stem cells (Nicklas et al., 2012).

During brain development, neural progenitors divide asymmetrically. These asymmetric divisions lead to an unequal inheritance of TRIM32 in only one of the two daughter cells. To induce neuronal differentiation, TRIM32 ubiquitiates c-Myc via its RING-finger domain and controls its protein stability. Interestingly, TRIM32 was discovered to interact with Ago-1. Furthermore, TRIM32 has also been shown to enhance the activity of let-7a which is upregulated during differentiation and responsible for the degradation of c-Myc as well. Therefore, protein degradation coordinated with translational inhibition via activation of microRNAs are the main pathways of TRIM32 to induce neuronal differentiation (Schwamborn et al., 2009).

2 Aim of the study

The overall aim of the study was to investigate the effect of the LRRK2 G2019S mutation on the balance between neural stem cell maintenance and differentiation in an age-dependent manner. Therefore, human neuroepithelial stem cells (NE cells) were used that carry the LRRK2 G2019S mutation and compared to WT cells with respect to their proliferation, differentiation, autophagy and apoptosis properties. Furthermore, we aimed on analyzing a potential interaction of LRRK2 WT and mutant with neural cell fate determinant TRIM32 and its effect on microRNA activity and mRNA expression levels.

The specific aims of this study were:

1) Effect of the LRRK2 G2019S mutation:

   a) How does the LRRK2 G2019S mutation affect the cell cycle of NE cells?

   b) Does the mutation have any influence on apoptosis rates during maintenance and differentiation?

   c) Does the mutation affect the degradation of mitochondria via autophagy during maintenance and differentiation state?

   d) Is senescence affected?

   e) How is TRIM32 distributed during maintenance and differentiation?

2) Interaction of LRRK2 and TRIM32:

   a) Interaction of LRRK2 and TRIM32 at exogenous and endogenous levels.

   b) Age-dependence of LRRK2 and TRIM32 expression levels and their interaction.

c) Does the complex contain the miRNAs Let-7a and miR-184 and mRNAs the *e2f1* and *dp1*?

d) Is the interaction RNA-dependent?

3 Materials and Methods

3.1 Materials

3.1.1 Companies

All general supplies, chemicals, solutions and laboratory equipment were purchased from the following companies:

Abcam plc, Cambridge, United Kingdom

Axon Medchem BV, Groningen, Netherlands

BD Bioscience, San Jose, USA

BioRad Laboratories GmbH, München, Germany

Carl Zeiss Vision GmbH, Aalen, Germany

Corning B.V. Life Sciences, Amsterdam, Netherlands

Dako Deutschland GmbH, Hamburg, Germany

Enzo Life Sciences GmbH, Lörrach, Germany

Fermentas, St. Leon-Roth, Germany

GenScript USA Inc., Piscataway NJ, USA

Gramsch Laboratories, Schwabhausen, Germany

Heraeus Sepatech GmbH, Osterode, Germany

Hirschmann Laborgeräte GmbH & Co. KG, Eberstadt, Germany

Invitrogen GmbH, Karlsruhe, Germany

Mettler-Toledo GmbH, Gießen, Germany

Millipore, Bedford, USA

New England Biolabs GmbH, Frankfurt am Main, Germany

PAA Laboratores GmbH, Pasching, Austria

PeproTech, Hamburg, Germany

Qiagen, Hilden, Germany

Raytest GmbH, Straubenhardt, Germany

Santa Cruz Biotechnology, Santa Cruz, USA

Sanyo, San Diego, USA

Sarstedt AG & Co, Nürnbrecht, Germany

Scientific Industries, Inc., New York, USA

Sigma-Aldrich Chemie GmbH, München, Germany

Thermo Fisher Scientific GmbH, Bremen, Germany

Vector Laboratories, Inc., Burlingame CA, USA

VWR International GmbH, Darmstadt, Germany

Weiss Labortechnik GmbH, Heroldsberg, Germany

3.1.2 Cultivation Media

Table 3.1: Stock solutions.

Stock Solution	Concentration	Companies
Ascorbic acid (AA)	20 mM	Sigma
B27 –Vitamin A	50 x	Invitrogen
Brain-derived neurotrophic factor (BDNF)	10 µg/µl	Sigma
CHIR	3 mM	Axon MedChem
Dibutyryladenosine cyclic monophosphate (dbcAMP)	100 mM	Sigma
Fibroblast growth factor 2 (FGF 2)	100 µg/ml	Peprotech
Fibroblast growth factor 8 (FGF 8)	100 µg/ml	Peprotech
Glial cell-derived neurotrophic factor (GDNF)	10 µg/µl	Sigma
L-glutamine	200 mM	PAA

N2	100x	Invitrogen
Penicillin/Streptomycin (P/S)	100x	PAA
Purmorphamin (ALX-420-045) (PMA)	10 mM	Enzo Life Science
TGF-β3	10 µg/ml	Peprotech

3.1.2.1 Human Embryonic Kidney cells (HEK293T) Culture

Modified Dulbecco's modified Eagle's medium MEM (DMEM) (PAA)

DMEM +++

L-glutamine	1:100
P/S	1:100
Fetal Calf Serum (PAA)	1:10

3.1.2.2 Neuroepithelial stem cell culture

Modified DMEM HAM's F12 (PAA) medium

HAM's F12

L-glutamine	1:100
P/S	1:100
B27 (–Vitamin A)	1:50

Modified Neurobasal (Gibco®) medium

  Neurobasal

  L-glutamine   1:100

  P/S   1:100

  N2   1:100

The basic medium (N2B27) for the NE cells consists of DMEM HAM'S F12 and Neurobasal medium 1:1.

Modified N2B27 medium for maintenance

  AA   1:133

  CHIR   1:1000

  PMA   1:20000

Modified N2B27 medium supporting differentiation into rosette cultures

  N2B27

  AA   1:100

  FGF2   1:500

  PMA   1:10000

Modified N2B27 medium supporting differentiation into ventral CNS neurons

N2B27

AA	1:100
FGF8	1:1000
PMA	1:10000

Modified N2B27 medium supporting maturation of differentiated cells

N2B27

AA	1:100
BDNF	1:1000
dbcAMP	1:200
GDNF	1:1000
PMA	1:10000
TGF-β	1:10000

3.1.3 Plasmids

Several plasmids were used for transfecting HEK293T cells. Those plasmids were gained in larger quantity by plasmid preparation in *Escherichia coli*.

Table 3.2: Plasmids for transfections of HEK293T cells.

Gen	Tag	Vector	Producer
EGFP	FLAG-HA	pIRESneo	Sven Diederichs
LRRK2-D2016A	FLAG	pCMV-Flag	F. Gillardon, Boehringer
LRRK2-G2019S	FLAG	pCMV-Flag	F. Gillardon, Boehringer
LRRK2-R1441H	FLAG	pCMV-Flag	F. Gillardon, Boehringer
LRRK2-WT	FLAG	pCMV-Flag	F. Gillardon, Boehringer
TRIM32	His	pDEST26	Invitrogen

3.1.4 Primers and PCR programs

mRNA primers and PCR program

All mRNA primers were purchased from Sigma Aldrich.

Table 3.3: mRNA primers for RT-qPCR.

Primer	Sequence (5' → 3')
E2F1 for	ATTGCCAAGAAGTCCAAGA
E2F1 rev	TTCAAGCCGCTTACCAAT
TRIM32 for	GCATCCAGGAAGAGCTAG
TRIM32 rev	CTCTACCACTTGACTGTTG
GAPDH for	ACAATGAATACGGCTACAG
GAPDH rev	GGTCCAGGGTTTCTTACT
p53 for	ATTGGGACCATCCTGGCTGTAG
p53 rev	CGAGGCTGATATCCGACTGTGA
p21 for	CTGTCTTGCACTCTGGTGTCTGA
p21 rev	CCAATCTGCGCTTGGAGTGA
Cdkn2d (p19) for	TGTTCGGAAGTGTTG
Cdkn2d (p19) rev	CAGGGCATTGACATCAGCACC

p16 for	CTGCCCACGCACCGAATA
p16 rev	TGCAGCACCACCAGCGTGTC
Ago2 for	CAGTGCGTGCAGATGAAGAA
Ago2 rev	ATGGACGTCTGCTCCCAGAA
TFDP1 for	ACACCCCCAGCACTCACTTT
TFDP1 rev	GGCCCTTGCCATTCTTCTCT

Table 3.4: RT-qPCR programm.

Initial denaturation	Denaturation	Primer annealing	Elongation	Cycle Number
95 °C, 2 min	95 °C, 20 s	58 °C, 30 s	72 °C, 10 s	45

3.1.4.1 MicroRNA primers and PCR program

All microRNA primer sets were purchased from Exiqon.

Table 3.5: Utilized microRNA primer sets for RT-microRNA PCR.

Primer Set	Target Sequence (5' → 3')
hsa-let-7a	UGAGGUAGUAGGUUGUAUAGUU
hsa-miRNA-184	UGACGGAGAACUGAUAAGGGU
hsa-snU6	CTGCGCAAGGATGACACGCA

Table 3.6: RT microRNA PCR program.

Process Step	Settings
Polymerase Activation / Denaturation	95 °C, 10 min
Amplification	95 °C, 10 s 60°C, 1 min
Amplification Cycles	45

3.1.5 Antibodies

Table 3.7: Primary and secondary antibodies for specific protein detection in western blots (WB) or Immunofluorescence stainings (IF).

Antigen	Antibody source	Application	Clone	Company
Alexa Fluor® 488 anti-mouse IgG (H+L)	Goat	IF: 1:1000		Molecular Probes (Invitrogen)
Alexa Fluor® 488 anti-rabbit IgG (H+L)	Goat	IF: 1:1000		Molecular Probes (Invitrogen)
Alexa Fluor® 488 anti-rat	Goat	IF: 1:1000		Molecular Probes (Invitrogen)
Alexa Fluor® 568 anti-mouse IgG (H+L)	Goat	IF: 1:1000		Molecular Probes (Invitrogen)
Alexa Fluor® 568 anti-rabbit IgG (H+L)	Goat	IF: 1:1000		Molecular Probes (Invitrogen)

Alexa Fluor® 568 anti-rat	Goat	IF: 1:1000		Molecular Probes (Invitrogen)
CD133 (Prominin-1)	Rat	IF: 1:400	13A4	Millipore
Cleaved Caspase3	Rabbit	IF: 1:200	ASP175	Cell Signaling Technology
COX IV	Rabbit	IF: 1:1000		Abcam
ECL-anti-mouse	Sheep	WB: 1:1000		GE Healthcare
ECL-anti-rabbit	Donkey	WB: 1:1000		GE Healthcare
FLAG M2	Mouse	WB: 1:800	M2	Sigma
GAPDH	Rabbit	WB: 1:1000		Abcam
Ki67	Rabbit	IF: 1:100		Vector Labs
Lamp1	Mouse	IF: 1:100	H4A3	Abcam
LRRK2	Rabbit	WB: 1:50	MJFF2 (c41-2)	Epiomics/Abcam
p16 INK4A	Mouse	IF: 1:100	1E12E10	Santa cruz
PH3	Mouse	IF: 1:100	6G3	New England Biolabs

TRIM32	Rabbit	WB: 1:600		Gramsch Laboratories
TRIM32	Rabbit	IF: 1:400		Gene Script

3.1.6 Software

Table 3.8: Software

Software	Provider	Application
Photoshop CS3	Adobe	image editing
Excel	Microsoft	creation of diagrams, statistical analysis
ImageJ	NIH	image processing
ZEN 2009	Zeiss	imaging by confocal laser scanning microscopy
AxioVision	Zeiss	imaging by epi-fluorescence microscopy
ND-1000 V 3.7.1	NanoDrop	BCA protein sample analysis
Bio-Rad iQ5	BioRad	melt curve analysis

3.2 Cell Culture

3.2.1 Culture of HEK293T cells

The HEK293T cell line was cultured on 10 cm dishes (BD Falcon) in DMEM +++ growth medium. Cells were incubated at 37 °C and 5 % CO_2. At a confluency of approximately 80-90 % the cells were split. Therefore, cells were detached and homogenized by pipetting up and down with a 10 ml pipette. 1ml cell suspension was transferred to a new 10 cm dish containing 7 – 8 ml DMEM+++.

3.2.2 Transient transfection

Transient transfection describes the temporal introduction of additional DNA into cells that is not integrated into the genome and is expressed for a certain period of time. Therefore, HEK293T cells were grown to a confluency of 70 %. For one 10 cm dish 10 µg of plasmid DNA were mixed with 1 ml serum-free DMEM and 20 µl TurboFect (Fermentas). After 20 min incubation at room temperature (RT) the mixture was added drop wise to each plate and the cells were incubated at 37 °C and 5 % CO_2 for 48 h.

3.2.3 Neuroepithelial stem cell (NE cell) culture

For *in vitro* studies, NE cells were received from the lab of Hans R. Schöler (MPI). These cells were generated by reprogramming fibroblast into induced pluripotent stem cells, which were subsequently differentiated into multipotent NE cells (Reinhardt et al, 2013). In this study wildtype and mutant NE cells with a LRRK2 G2019S mutation were utilized.

3.2.3.1 Cultivation of NE cells

Human NE cells were cultured on Matrigel-coated (hES qualified Matrigel, BD Bioscience) 12 well plates in N2B27 medium supplemented with 150 µM AA, 3 µM CHIR and 0.5 µM PMA to keep them under maintenance conditions. Cells were incubated at 37 °C and 5 % CO_2 and the medium was changed every two or three days.

3.2.3.2 Passaging of NE cells

NE cells were split once a week 1:10 – 1:25 according to the cell density. Therefore, the growth medium was removed and the cells were incubated with 250 µl StemPro® Accutase® (Invitrogen) for 2-4 min until the cells started to detach. The dissociation reagent was stopped with 2 ml Stop solution (10 % BSA in DMEM) and the cells were transferred to a Falcon tube for centrifugation (900 rpm, 3 min). The stop solution was discarded and the cell pellet was resuspended in growth medium before plating on Matrigel-coated 12-well plates.

3.2.3.3 Formation of neural rosettes

The exchange of certain small molecules results in a differentiation of the neuralepithelial stem cells into a desired cell type. Neural rosettes were obtained by replacing CHIR through 20 µg/ml fibroblast growth factor 2 (FGF2) 200 µM AA and 1 µM PMA. After 4 days of cultivation under these conditions cells were fixed and further analyzed by immunofluorescence stainings.

3.2.3.4 Differentiation into ventral midbrain neurons

The differentiation of NE cells into ventral midbrain neurons consists of two phases. First, the maintenance medium was replaced by N2B27 medium with 100 ng/ml FGF8, 1 µl PMA and 200 µM AA for 7 days with a medium change every two or three days. On the eighth day the medium was exchanged to a maturation medium that contained N2B27, 10 ng/ml BDNF, 10 ng/ml GDNF, 1 ng/ml TGF-β3, 200 µM AA, 500 µM dbcAMP. Again the medium was changed every two or three days. During the first seven days after induction of the differentiation, the cells were split 1:5 if necessary.

3.2.3.5 Freezing of NE cells

For long-term storage, NE cells were first detached with Accutase and collected in a falcon for centrifugation (900 rpm, 3 min) as described in 3.2.3.2. The pellet was resuspended in maintenance growth medium supplemented with 10 % DMSO. One well of a 12-well plate was frozen in one cryotube and transferred to a liquid nitrogen tank.

3.2.3.6 Thawing of NE Cells

Frozen cells were rapidly thawed in freshly prepared maintenance medium and one cryotube was plated onto two wells of a 12 well plate. After two days the medium was changed.

3.3 Protein biochemical methods

3.3.1 Cell lysis

For cell lysis the growth medium was taken off and the cells were detached using 10 ml 1x PBS and transferred to a Falcon tube. After 10 min of centrifugation (1250 rpm, 4 °C) the pellet was dissolved in 1 ml 1x PBS and transferred into an 1,5 ml Eppendorf tube for centrifugation (2 min, 6000 rpm, 4 °C).

Depending on its size, the cell pellet was resuspended in 400 – 600 µl of 2 % Triton X-100 lysis buffer (2 % Triton X-100 (Sigma), 1x Complete mini protease Inhibitor (Roche), 1x PBS) and incubated for 30 min at 4 °C on an overhead shaker. Afterwards the samples were centrifuged for 30 min (13000 rpm, 4 °C) to separate the solvent protein from the solid cell debris.

To check the transfection efficiency, 30 – 50 µl of the supernatant was diluted in 2x sample buffer. Subsequently, the lysate was boiled for 15 min at 95 °C and stored at -80 °C until further analysis. The remaining supernatant was utilized for immunoprecipitation.

3.3.2 Brain lysis

For brain lysis the same lysis buffer was used as in 3.3.1. The brains were shredded first by pipetting and afterwards by passing through a needle. The lysates were incubated for 1 h at 4 °C on an overhead shaker and processed further as in 3.3.1.

3.3.3 BCA-Assay

Protein concentrations were determined by using the BCA^{TM} Protein Assay Kit (Thermo Scientific). This method links two chemical reactions in an alkaline medium with a highly sensitive and selective colorimetric detection. First Cu^{2+} is reduced to Cu^{1+} by the proteins present in the sample. The Cu^+ ions are then chelated by two bicinochinic acid (BCA) molecules forming an intense purple-colored reaction product. The absorbance of this complex can be detected at a wavelength of 562 nm and is proportional to the protein concentration. The assay was performed according to manufacturer's instructions the adsorption of the solution was measured with NanoDrop (ND-1000).

3.3.4 Immunoprecipitation (IP)

The interaction of a certain protein with potential interaction partners was determined with an IP. Therefore, the supernatant of the brain lysis or cell lysis was incubated with 5 µl precipitation antibody for 4 h at 4 °C on an overhead shaker. Meanwhile, protein-G-Agarose beads (GE Healthcare) were washed three times with 2 % Triton X-100 in 1x PBS. After 4 h, the whole cell lysate was added to the washed beads and incubated overnight at 4 °C on the overhead shaker.

On the following day the beads were washed three times with 0.2 % Triton X-100 in 1x PBS (13000 rpm, 1 min at 4 °C). To elute bound proteins from the beads, the beads were boiled in 2x sample buffer at 95 °C for 15 min while shaking. For detection of LRRK2, samples were cooked for only 1 min. The beads were centrifuged for 5 min at 13000 rpm and the supernatant was taken off for further analysis by SDS-PAGE or temporary storage at – 80 °C. If the samples were used

for RT-qPCRs they were not diluted with 2x sample buffer but directly taken for the reverse transcription.

3.3.5 SDS polyacrylamide gel electrophoresis (SDS-PAGE)

Proteins were separated according to their molecular weight by SDS-PAGE. The SDS-detergent binds to the proteins causing the loss of their native conformation and giving them a negative charge that allows their migration in the discontinuous electric field in proportion to the protein size. The total concentration of the acryl amide determines the pore size of the gel. In this study polyacrylamide gels with 7.5 % and 10 % concentration were used for analysis. The gels were prepared in 1.0 mm cassettes (Invitrogen) and the SDS-PAGE was performed by using XCell SureLock® Mini-Cell (Invitrogen) filled with 1x running buffer. Generally, 10 µl of the protein lysate and 20 µl of the IP were loaded into the gel slots. For size reference a standard molecular weight marker (Page-Ruler[TM] Plus Prestained Protein Ladder, Fermentas) was used. Electrophoresis was performed at 160 V for 80 min.

Table 3.9: Volume of the ingredients for 1 separation and 1 stacking gel.

Separation Gel 7 %	Separation Gel 10 %	Stacking Gel	Ingredient
4 ml	3.3 ml	1.5 ml	H_2O
-	-	0.624 ml	1.5 M Tris-HCL, pH 6.8
2 ml	2 ml	-	1.5 M Tris-HCl, pH 8.8

2 ml	2.7 ml	0.374 ml	30 % Acryl amide
0.05 ml	0.05 ml	0.01 ml	10 % APS
0.005 ml	0.005 ml	0.004 ml	TEMED

10x Running Buffer (ad 1 l H$_2$O)

30.3 g Tris (Applichem)

144.2 g Glycine (Applichem)

3.3.6 Western Blot

Separated proteins were transferred from the SDS-gel onto a nitrocellulose membrane (Amersham Hybond^{TM} ECL^{TM}) by Western blotting for further analysis. Based on the wet-transfer method the gel, the membrane, Whatman papers and sponges had to be equilibrated in blotting buffer before starting the procedure. To obtain an efficient transfer from the gel onto the membrane the following sandwich was built in the Blotting Module (XCell II^{TM} Invitrogen): minus pole – 2 sponges – 2 Whatman paper – gel – membrane – 2 Whatman paper – 2 sponges – plus pole. The module was fixed within the Mini-cell system and filled up with blotting buffer. The transfer was performed at 4 °C with 350 mA for 70 min.

After the transfer, the membrane was reversibly stained with Ponceau-S solution to verify efficient transfer and equal loading of the samples. The staining was reversed by washing in ddH$_2$O and the membrane was incubated for 1 h with blocking solution to block unspecific binding sites. Afterwards, the membrane was incubated with the primary antibody diluted in antibody solution overnight at 4 °C. On

the next day, the membrane was washed three times for 5 min in washing solution to remove unbound antibodies. Afterwards, it was incubated with the secondary antibody linked to horseradish-peroxidase for 1 h at RT and washed three times for 5 min in washing solution.

Detection of bound antibodies was performed using the ECL Super signal West Pico Chemiluminescent Substrate Kit (Thermo scientific). A chemiluminescence signal can be detected due to the activity of the horseradish-peroxidase which catalyzes the oxidation of luminol in the presence of H_2O_2. The emitted light was detected using the STELLA Imaging System (RayTest) and images were further analyzed with Adobe Photoshop CS3.

Blotting Buffer (in H_2O)

1x Running Buffer (without SDS)

20 % MeOH

0.01 % SDS

Ponceau S

0.01 % Ponceau S

5 % Acetic acid

Blocking Solution (in 1x PBS)

5 % Milk powder (Carl Roth)

0.2% Tween-20 (Applichem)

Antibody Solution (in 1x PBS)

5 % Milk powder

0.02% Tween-20

Washing Solution (in 1x PBS)

0.02 % Tween-20

3.3.7 Senescence β-galactosidase staining

To investigate the appearance of senescence in later passages of the cells a senescence beta-galactosidase staining kit (Cell signaling Technology®) was used. During senescence the lysosomes overexpress and accumulate an enzyme called beta-galactosidase. The hydrolysis of ß-galactosides presented by the staining solution of the kit into monosaccharides leads to the formation of a blue color in an environment of pH 6.

Cells were seeded on cover slips in 24-well plates and the kit was utilized as described in the manufacturer's instructions. After fixation of the cells, the cover slips were rinsed twice with 1x PBS. The staining solution was mixed and applied to the cells overnight at 37 °C. The next day the cells were analyzed using a light microscope for the development of blue color.

3.3.8 Brightfield imaging

Beta-galactosidase staining (3.3.7) was analyzed by bright field imaging using the Axioplan 2 microscope (Zeiss) and Metamorph software.

3.4 Molecular biological methods

3.4.1 cDNA synthesis

For investigation of mRNA expression levels, RNA was isolated from wildtype or mutant NE cells using the RNeasy kit (Quiagen) The freshly isolated RNA or a part of the IPs (3.3.4) was then transcribed into cDNA by reverse transcription (RT). Therefore, 10 µl RNA were mixed with 1 µl random primer (Sigma) and 1 µl dNTP

Mix (10 mM). After incubation for 4 min at 70 °C, the mix was cooled down on ice. Next, 8 µl of a Master Mix (4 µl 5x First-Strand Buffer, 2 µl 0.1 M DTT, 1 µl RNAse Inhibitor and 1 µl RT-Enzyme (SuperScript)) were added, followed by incubation of the reaction mix for 90 min at 42 °C and 15 min at 70 °C. The cDNA was subjected to real time qPCR or stored at -20 °C.

3.4.2 Real time-quantitative PCR (RT-qPCR)

RT-qPCR was used to investigate differences in expression levels of various mRNAs. With this method a fluorescence signal that is proportional to the amount of PCR product is measured, after each cycle of amplification.

Therefore, the cDNA synthesized in 3.4.1 was used as a template for amplification. The RT-qPCR was performed according to the PeQLab SyberGreen protocol with 150 % primer volume.

Master Mix

2.7 µl H_2O

0.9 µl forward Primer

0.9 µl reverse Primer

7.5 µl SyberGreen (PeQLab)

3 µl Template

The reaction was performed in triplicates with 15 µl per sample in a 96 well-plate (iCycler iQ^{TM} PCR Plate, BioRad). Before starting the PCR reaction (Table 3.4) the plate was sealed with a microseal (Microseal B Adhesive Sealer MSB-1001, BioRad) and centrifuged.

The cycle threshold (CT) indicates the number of cycles at which the fluorescence of the sample exceeds the threshold. Hence, the CT values were used for calculation in Microsoft Excel and the melting curves were analyzed with BioRad iQ 5.

3.4.3 RT microRNA PCR

Expression levels of miRNAs bound to proteins that were precipitated by an IP (3.3.4) from brain lysates were analyzed using the miRCURY LNA^{TM} Universal RT microRNA PCR (Exiqon). First, a reverse transcription was performed to generate templates for the miRNA real-time PCR assays. Therefore, 4 µl 5x reaction buffer, 12 µl nuclease-free water, 2 µl enzyme mix and 2 µl template (IP) were mixed gently and incubated for 60 min at 42 °C. This was followed by heat-inactivation of the reverse transcriptase for 5 min at 95 °C and cooling down at 4 °C for storage.

The second step comprised the real-time qPCR according to the Exiqon protocol. Therefore, the cDNA generated in the first step was diluted 1:10 with nuclease free water and 8 µl of it were mixed with 5 µl SYBR Green master mix (PeQLab), 1 µl forward Primer, 1 µl reverse Primer. The reaction was done in triplicates with a reaction volume of 20 µl per well in a 96-well plate using the recommended RT-qPCR program from Exiqon (Table 3.6). The CT values were used for calculation in Microsoft Excel.

3.5 Immunofluorescence

3.5.1 Immunofluorescence staining

For immunofluorescence stainings cells were seeded on Matrigel-coated glass cover slips in a 24-well plate. Cells were fixed with 4 % PFA (in 1x PBS) for 15 min and washed three times with 1x PBS. Next, the cell membranes were permeabilized with 0.05 % Triton X-100 in 1x PBS for 3 min on ice. After three washing steps, the cells were blocked with 10% FCS in 1x PBS for at least 1 h at room temperature. The primary antibody was diluted in 10 % FCS (in 1x PBS) and subjected to the cells for 90 min in a wet chamber. After three washes of 5 min with 1x PBS, the cells were incubated for 60 min with the secondary antibody and Hoechst in the wet chamber. The cells were washed three times with 1x PBS and once with milliQ H_2O before mounting the cover slips on a glass slide upside down with mounting medium (DAKO AquaMount). Glass slides were stored in the cold room at 4 °C.

3.5.2 Fluorescence microscopy

Immunofluorescence stainings were analyzed either by confocal microscopy (Axio Imager.Z2, LSM710 detector, Zeiss) or fluorescence microscopy (Axio Imager M, fluorescence microscope).

ZEN software (Zeiss) was used as imaging software for confocal pictures whereas Visiview software (Visitron System) was utilized for the fluorescence microscopy. Images were processed with Adobe Photoshop CS3 or ImageJ. Statistical analyses were performed using Microsoft Excel.

3.5.3 Co-localization in ImageJ

Equal quantity of representative confocal pictures were taken and further analyzed with an ImageJ plug in called JACoP. As a representative indicator for co-localization, the Pearson correlation coefficient was chosen. This coefficient is mainly used to measure the strength of linear relationship between two variables. The correlation coefficient is especially preferred for a first identification of diverse relationships and for investigation of complex overlays. The coefficient reaches from 1 to -1 whereat 1 indicates a complete positive correlation and -1 a negative correlation, zero stands for no correlation (Bolte and Cordelières, 2006).

4 Results

4.1 Differentiation of neuroepithelial stem cells (NE cells) into neural rosettes

NE cells appear during early development of the embryo. These multipotent cells are able to differentiate into neural tube as well as neural crest lineages *in vivo* and *in vitro* (Patthey et al., 2009*;* Reinhardt et al., 2013). In order to verify their differentiation potential *in vitro,* differentiation into neural rosettes was induced by cultivation of NE cells in rosette formation medium supplemented with FGF2 for 4 days (Zhang et al., 2001).

Neural rosette cells express markers characteristic for ESCs and also NSCs markers. Therefore, they can give rise to cells with a fate towards the central nervous system (CNS) as well as the peripheral nervous system (PNS). Additionally, to their broad differentiation potential, they exhibit an extensive growth potential (Elkabetz et al., 2008).
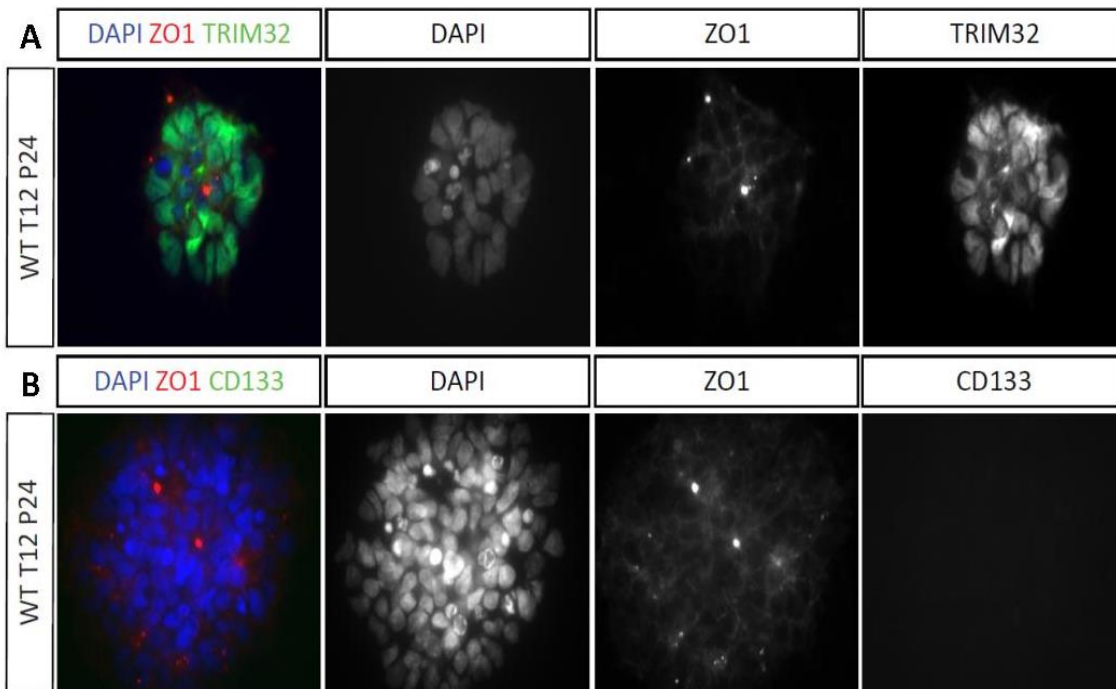
Figure 4.1: Differentiation of NE cells into neural rosettes. WT cells were cultured under differentiation conditions with 40 µg FGF2, 1µM PMA and 200 µM AA for 4 days to induce rosette formation. **(A)** Rosettes were stained for TRIM32 or **(B)** CD133 and co-stained with the apical marker ZO1.

Differentiation into rosettes was assayed by staining for ZO1, which acquires an asymmetric apical localization during neural fate induction (Elkabetz et al., 2008). TRIM32 has not been analyzed in neural rosettes before, but it is known to play a role during neuronal differentiation (Hillje et al., 2011; Schwamborn et al., 2009). TRIM32 was found to be mainly localized to the nucleus in neural rosettes but was also distributed throughout the cytoplasm (Figure 4.1A). The apical neural stem cell marker CD133 was not expressed in differentiated NE cells although it was recently shown to become similarly restricted to the apical membranes during neural induction as ZO1 (Figure 4.1B) (Elkabetz et al., 2008). CD133 is a membrane glycoprotein

located to membrane protrusions and it is suggested to play an important role in key stem cells functions (Shmelkov et al., 2005).

4.2 Phenotype of the LRRK2 Mutation G2019S

4.2.1 Cell cycle and apoptosis under maintenance conditions

The LRRK2 mutation G2019S has been associated with sporadic as well as familial Parkinson's disease (PD). To investigate the impact of LRRK2 G2019S mutation on ageing, WT and LRRK2-G2019S expressing NE cells were cultivated over several passages to simulate ageing. Passages (p) 18 and 23 were fixed. To study possible differences in cell cycle or apoptosis, cells were stained for either Ki67 and PH3 or Cleaved Caspase 3 (Figure 4.2 and 4.3A).

Quantification of Ki67+ cells revealed that the number of cells being in the cell cycle is similar between WT and LRRK2 mutant cells in both passages (WT p18 3.5 % n > 3000 cells, p23 9.96 % n > 2500 cells; LRRK2 p18 2.56 % n > 2800 cells, p23 15.05 % n > 1800 cells) (Figure 4.2E and 4.3E). The number of PH3+ cells was also unchanged at passage 18 (WT 2.89 % n > 3000 cells; LRRK2 2.32 % n > 3000 cells) (Figure 4.2E), while it was significantly increased at passage 23 in WT compared to mutant cells (WT 2.82 % n > 2500 cells; LRRK2 1.53 % n > 1800 cells; $p < 0.05$) (Figure 4.3E).
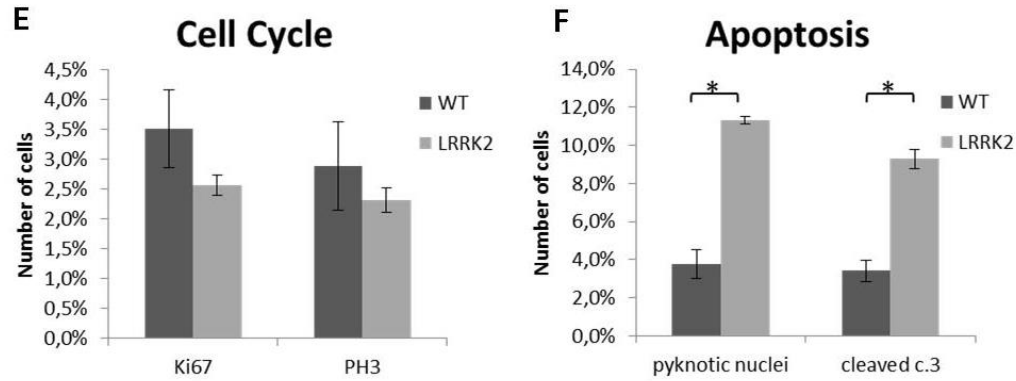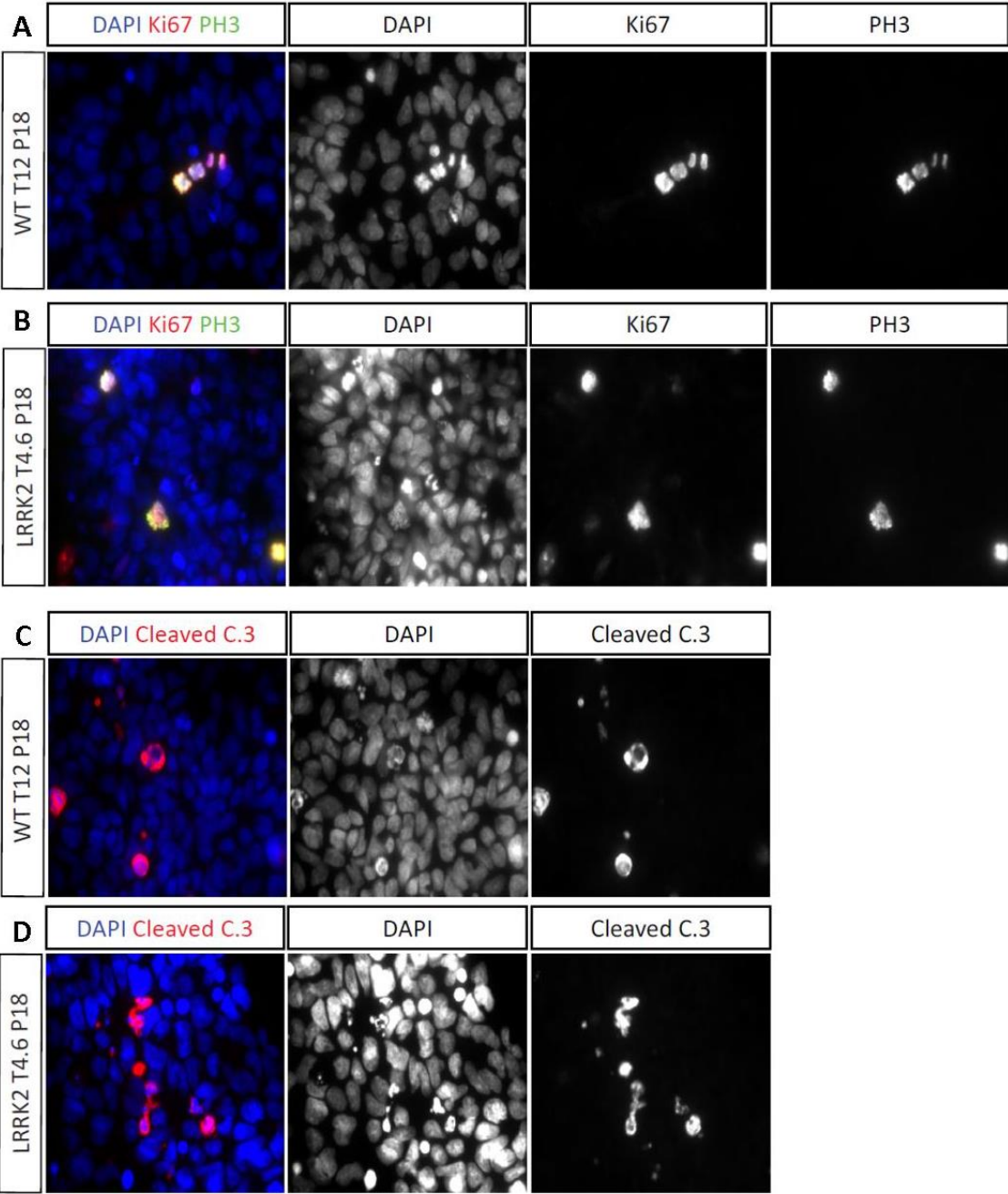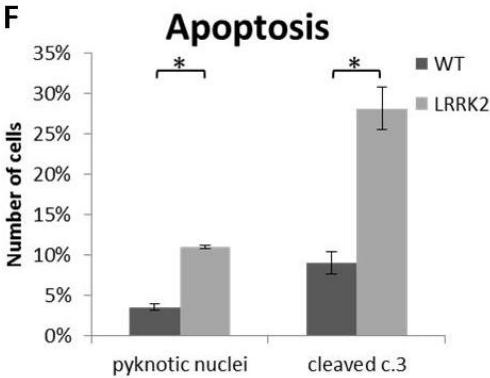
Figure 4.2: Analysis of cell cycle and apoptosis in WT and LRRK2 mutant NE cells at p18. P18 NE cells were cultured for 2 days on matrigel-coated plates in maintenance medium. **(A, B)** Fluorescence stainings using Ki67- and PH3-antibodies were done to label cells in the cell cycle. Nuclei were counterstained with Hoechst. **(C, D)** Fluorescence stainings using a Cleaved Caspase 3-antibody were done to label cells undergoing apoptosis. Nuclei were counterstained with Hoechst. **(E)** Quantification of Ki67+ and PH3+ cells in WT and LRRK2 mutant cells. **(F)** Quantification of Cleaved Caspase 3+ cells as well as pyknotic nuclei (mean ± s.e.m.; Mann-Whitney U Test P-Value: *p < 0.05).

In contrast, the difference in the amount of apoptotic cells was more obvious with a 3 fold higher apoptosis rate in mutant compared to WT cells (pyknotic nuclei: WT p18 3.78 % n > 3000 cells, LRRK2 p18 11.31 % n > 2800, p < 0.05; WT p23 3.53 % n > 2500 cells, LRRK2 p23 11.02 % n > 1800 cells, p < 0.05; Cleaved Caspase 3+: WT p18 3.4 % n > 2800, LRRK2 p18 9.28 % n > 2800, p < 0.05; WT p23 9.01 % n > 2600, LRRK2 p23 28.12 % n > 2100, p < 0.05) (Figure 4.2E, F and Figure 4.3E, F).
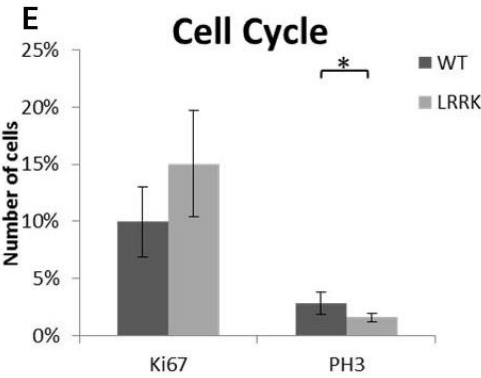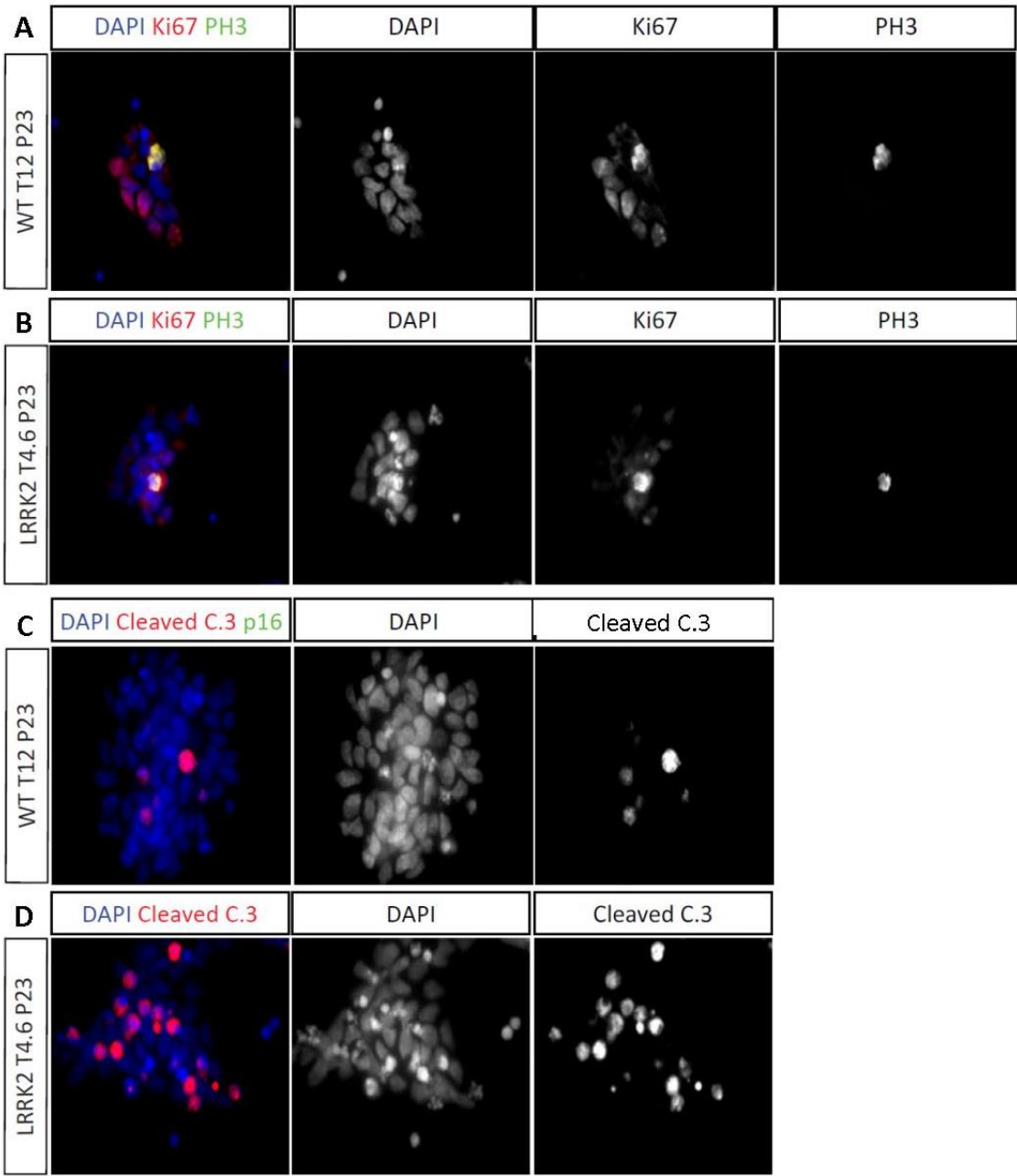
Figure 4.3: Analysis of cell cycle and apoptosis in WT and LRRK2 mutant cells NE at p23. P23 NE cells were cultured for 2 days on matrigel-coated plates in maintenance medium. **(A, B)** Fluorescence stainings using Ki67- and PH3-antibodies were done to label cells in the cell cycle. Nuclei were counterstained with Hoechst. **(C, D)** Fluorescence stainings using a Cleaved Caspase 3-antibody were done to label cells undergoing apoptosis. Nuclei were counterstained with Hoechst. **(E)** Quantification of Ki67+ and PH3+ cells in WT and LRRK2 mutant cells. **(F)** Quantification of Cleaved Caspase 3+ cells as well as pyknotic nuclei (mean ± s.e.m.; Mann-Whitney U Test P-Value: *p < 0.05).

4.2.2   Apoptosis under differentiation conditions

In order to compare the cell cycle and apoptosis under differentiation conditions of WT and LRRK2 G2019S mutant cells, NEs at p18 were kept under differentiation conditions for differentiation into ventral midbrain neurons, for 10 days and analyzed for apoptosis rates and cell cycle markers. PH3+ and Ki67+ cell exhibited slight differences between the cells (Ki67+: WT 1.62 % n > 900, LRRK2 1.02 % n > 900; PH3+: WT 1.95 % n > 900, LRRK2 1.42 % n > 900) and consistently indicate the high apoptosis levels in G2019S mutated NEs (Cleaved Caspase 3+: WT 5.24 % n > 1000, LRRK2 6.24 % n > 1000 (Figure 4.4). This experiment was done once, therefore no statistical evaluation is included and further experiments are necessary to verify these results.
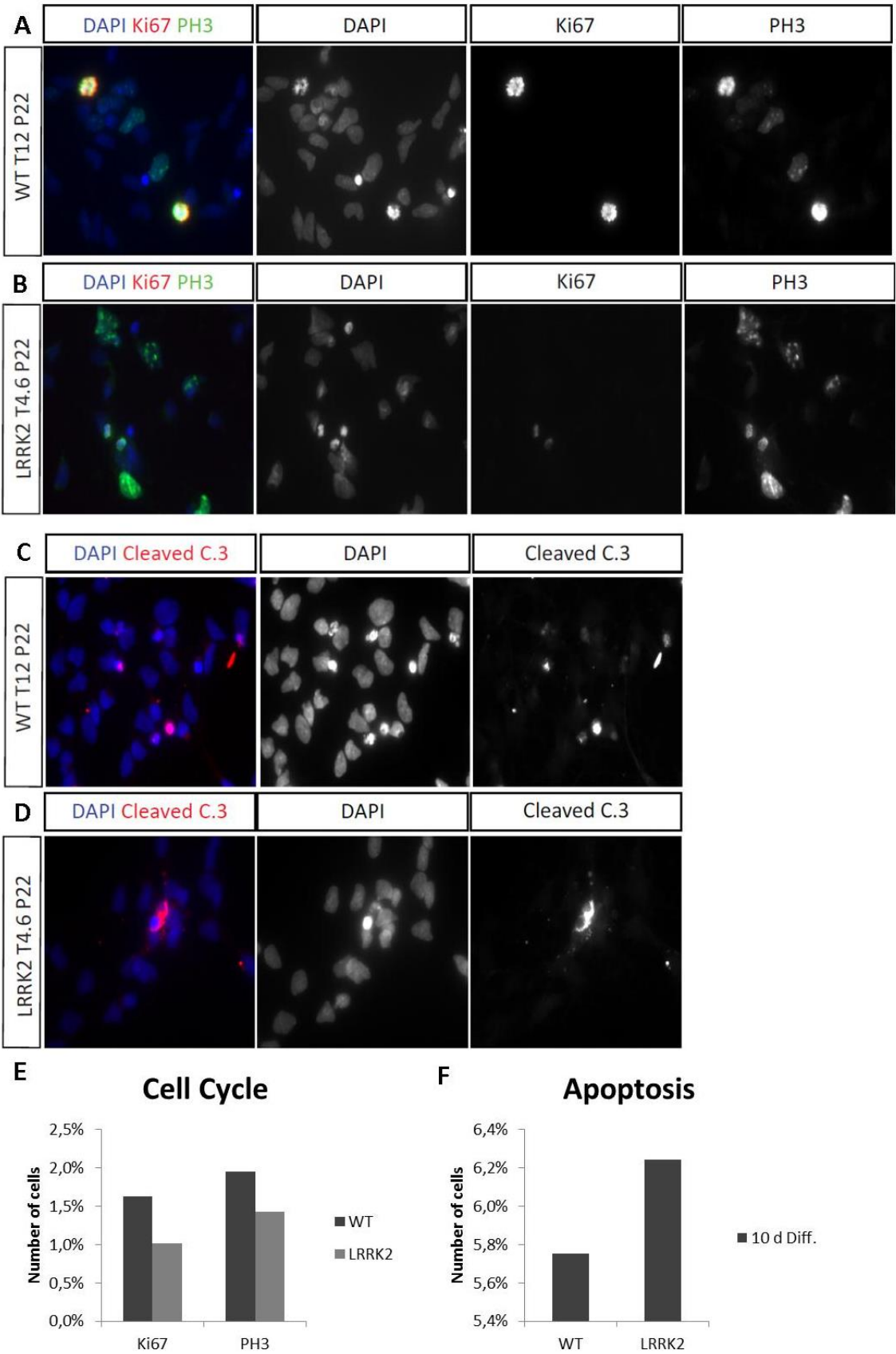
Figure 4.4: Evaluation of cell cycle and apoptosis in LRRK2 mutant cells during the first steps of differentiation. WT and LRRK2 G2019S mutant cells were cultured in presence of differentiation-inducing factors for seven days followed by 3 days in maturation medium. **(A, B)** Fluorescence staining with Ki67- and PH3-antibodies, Nuclei were counterstained with Hoechst. **(C, D)** Fluorescence staining of Cleaved Caspase 3. **(E)** Quantification of Ki67+ and PH3+ cells in WT and LRRK2 mutant cells. **(F)** Quantification of Cleaved Caspase 3+ cells.

Furthermore, NE cells of p18 were keep under differentiation conditions for 2 weeks and analyzed for apoptosis rates (Cleaved Caspase 3+: WT 10.61 % n > 2300, LRRK2 26.15 % n > 1900; p>0.05). Comparision of the p18 NE cells kept under maintenance conditions and after two weeks differentiation exhibited a significant increase of apoptotic cells after differentiation (Cleaved Caspase 3+: WT p18 main 3.4 % n > 2800, WT diff. 10.61 % n > 2300, p>0.05; LRRK2 p18 main. 9.28 % n > 2800, LRRK2 diff. 26.15 % n > 1900; p>0.05,) (Figure 4.5C, D).
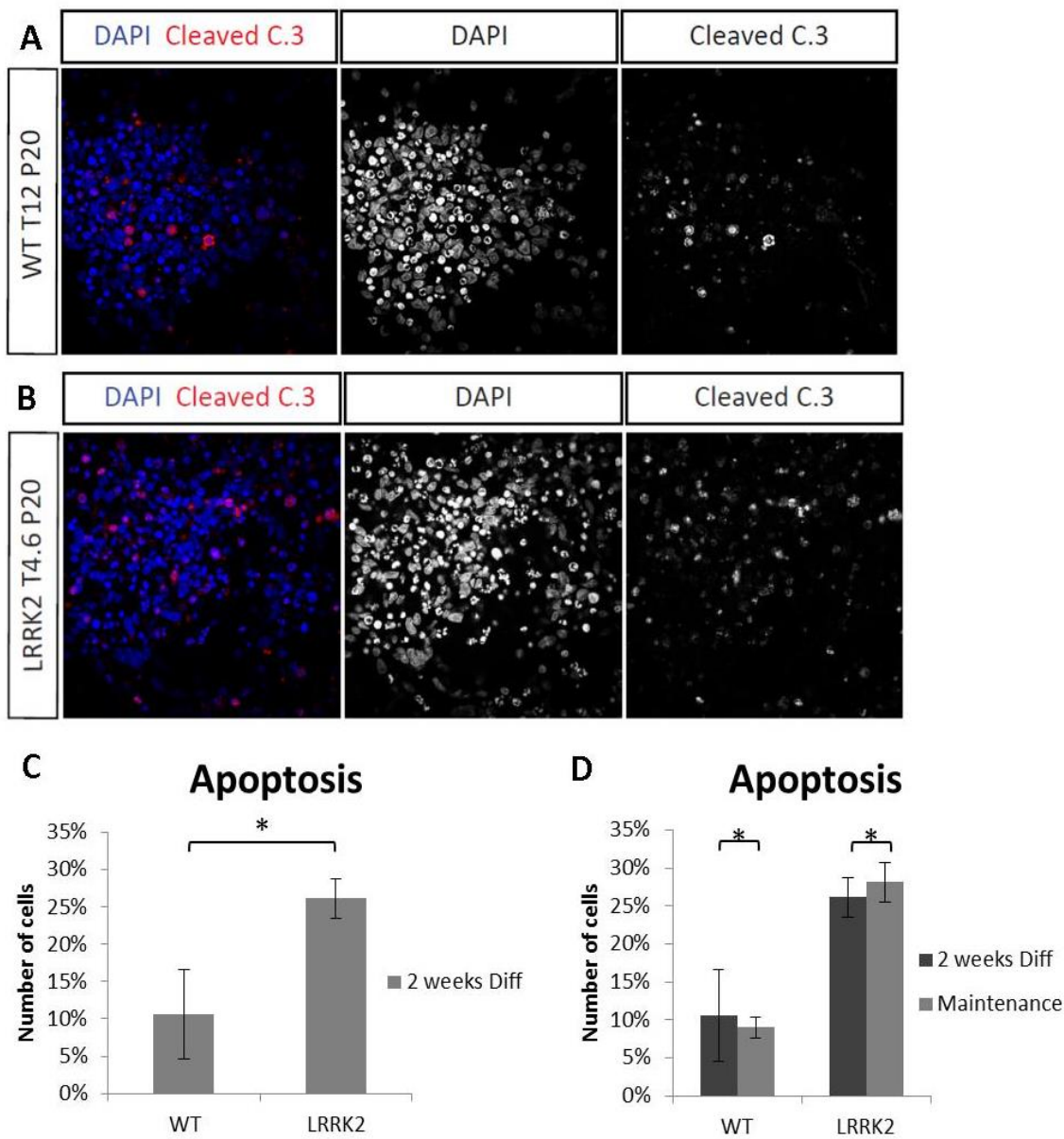
Figure 4.5: Apoptosis rate of WT and LRRK2 mutant cells two weeks after differentiation. (A, B) Immunofluorescence staining with Cleaved Caspase 3 to label apoptotic cells. **(C)** Quantification of Cleaved Caspase 3+ cells to label in WT and LRRK2 mutant cells. **(D)** Comparison of the fraction of Cleaved Caspase 3+ cells in WT and LRRK2 mutant cells under maintenance and differentiation conditions (mean ± s.e.m.; Mann-Whitney U Test; P-Value: *p < 0.05).

4.2.3 Autophagy

During ageing, the levels of damaged or defective mitochondria, due to errors in the mitochondrial genomes or reactive oxygen species (ROS), increase within the cell (Wallace et al., 2010). To prevent accumulation of dysfunctional mitochondria, which would lead to the initiation of apoptotic signaling cascades, cells induce recycling of the damaged mitochondria via a process called mitophagy (Kroemer et al., 2010). Autophagy is the overall term of cellular degradation of proteins or dysfunctional compartments through lysosomes. This process has been shown to decline during ageing, which results in the accumulation of defective cell organells that could ultimately lead to diseases like Parkinson's or Alzheimer's disease (Lipinski et al., 2010).

To determine the influence of the LRRK2 mutation on the degradation of mitochondria during ageing, the co-localization of lysosomes and mitochondria was examined. As in the previous experiments, cells from passages 18 and 23 were used and stained for CoxIV (mitochondira marker) and Lamp1 (lysosomal marker).
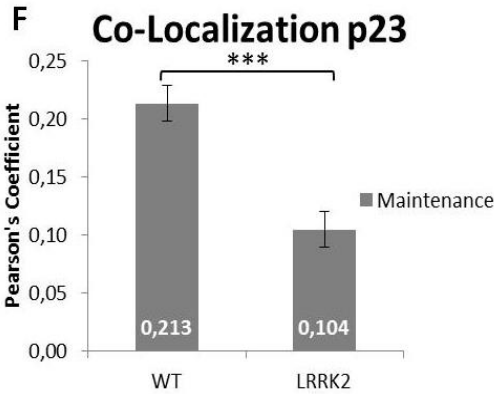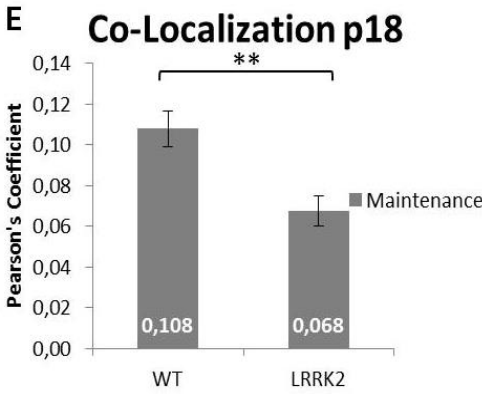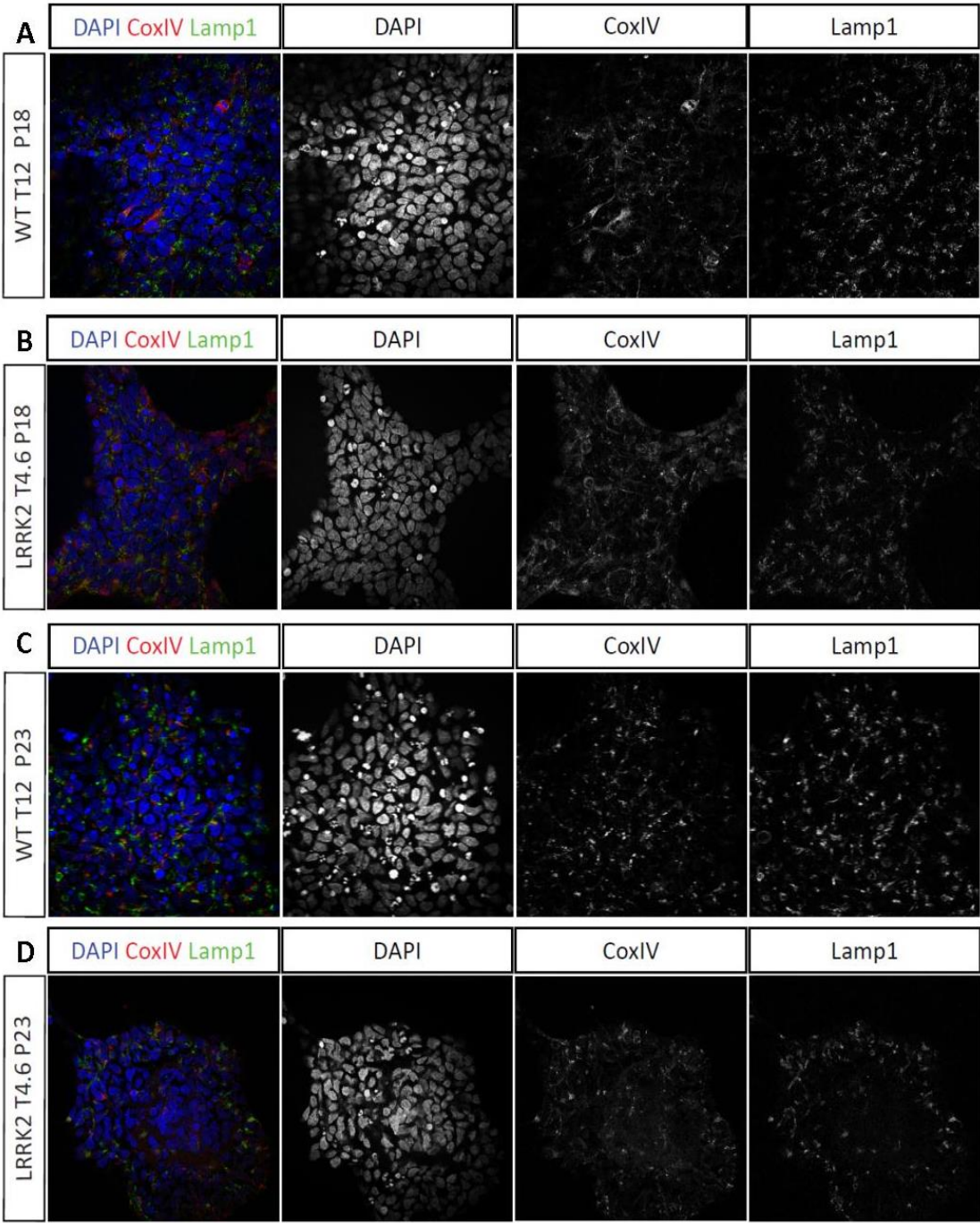
Figure 4.6: Co-Localization of mitochondria and lysosomes in WT and LRRK2 mutant NE cells at p18 and p23. NE cells at p18 and p23 were fixed and stained for CoxIV (mitochondrial marker) and Lamp1 (lysosomal marker). Images were analysed by Image J with the JACoP plug in. **(A, B)** Confocal pictures of WT and LRRK2 mutant cells to vizualize lysosomes and mitochondria at p18. **(C,D)** Confocal pictures of WT and LRRK2 mutant cells to vizualize lysosomes and mitochondria at p23. **(E, F)** The Pearson correlation coefficient was used to quantify the degree of co-localization and displayed a significant difference between WT and LRRK2 mutant cells (mean ± s.e.m.; Mann-Whitney U Test; P-Value: *$p < 0.05$; **$p < 0.005$, ***$p < 0.001$).

In both passages the co-localization of lysosomes and mitochondria was significantly increased in wildtype compared to LRRK2 mutant cells (Pearson coefficient: WT p18 0.1078, LRRK2 p18 0.0675, $p > 0.005$; WT p23 0.213, LRRK2 p23 0.104, $p > 0.001$, average of twelve pictures of each cell line) (Figure 4.6E, F). Furthermore, the degree of co-localization increased with higher passages of both WT and mutant cells. Moreover, the cells were differentiated for 2 weeks and stained for the same mitochondrial and lysosomal markers to determine the impact of differentiation on autophagy (Figure 4.8).

After differentiation, the overlap of lysosomes and mitochondria was significantly higher in WT cells compared to mutant cells (Pearson coefficient: WT 0.155, LRRK2 0.104, $p > 0.005$). In both cell types a highly significant increase of mitophagy was observed two weeks after differentiation induction compared to maintenance conditions (Pearson coefficient: WT p18 0.1078, WT diff. 0.155, $p > 0.05$; LRRK2 p18 0.0675, LRRK2 diff. 0.104, $p > 0.001$) (Figure 4.8E). However, not only the co-localization but also the shape of the organelles changed to a more punctate pattern (Figure 4.8A-D).
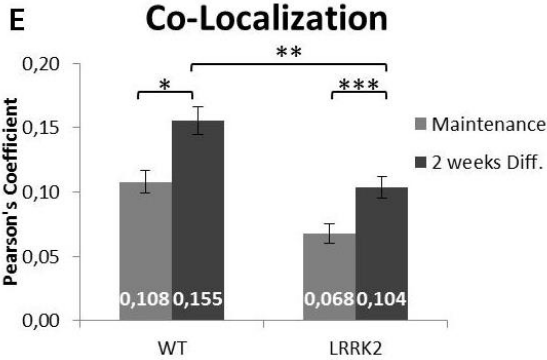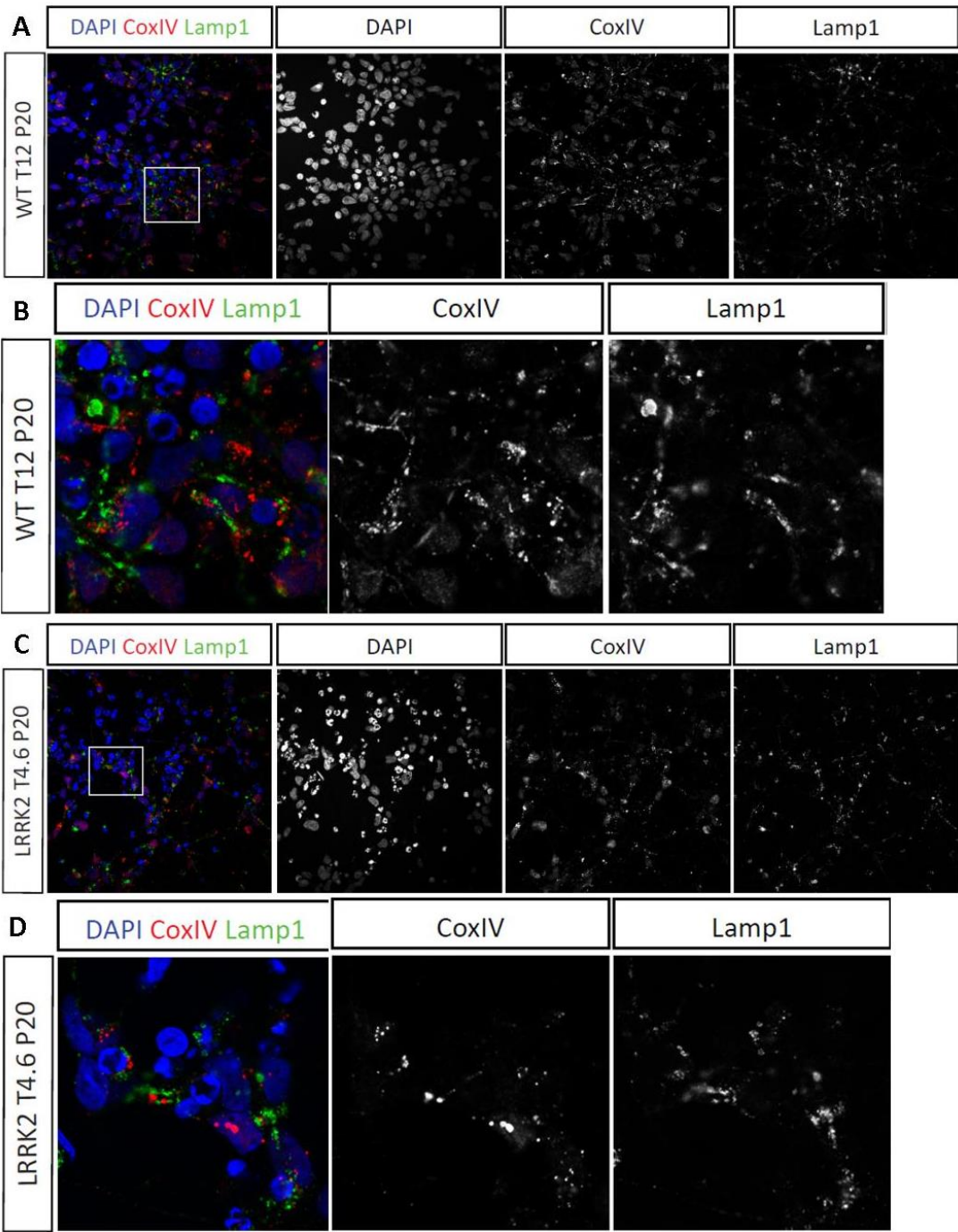
A DAPI CoxIV Lamp1 | DAPI | CoxIV | Lamp1
WT T12 P20

B DAPI CoxIV Lamp1 | CoxIV | Lamp1
WT T12 P20

C DAPI CoxIV Lamp1 | DAPI | CoxIV | Lamp1
LRRK2 T4.6 P20

D DAPI CoxIV Lamp1 | CoxIV | Lamp1
LRRK2 T4.6 P20

E Co-Localization

Figure 4.7: Quantification of the co-localization from mitochondria and lysosomes after differentiation. WT and LRRK2 mutant cells were differentiated for two weeks with the two step differentiation protocol. Afterwards the cells were fixed and stained for CoxIV and Lamp1. **(A, C)** Confocal pictures of WT and LRRK2 mutant cells were taken for analysis by Image J with the JACOP plug in. **(B,D)** Enlargements of chosen reagions demonstrate the overlap in higher resolution. **(E)** The Pearson's correlation coefficient was utilized to quantify the degree of co-localization and displayed a significant difference between WT as well as mutant cells under maintenance and differentiation Additionally, the difference between differentiated WT and LRRK2 cells was also significant. (mean ± s.e.m.; Mann-Whitney U Test; P-Value: *p < 0.05; **p < 0.005 ***p < 0.,001)

4.2.4 Senescence during ageing

Senescence describes an irreversible arrest of cell proliferation. Additionally to the cell cycle arrest, senescent cell exhibit changes in chromatin organization and gene expression. It is also described as a sort of tumor suppression and has powerful paracrine activities which is called senescence associated secretory phenotype (SASP). Furthermore, a change of the cell morphology and doubling of cell volume occur, but senescent cells remain viable and metabolically active. Reasons for this transformation are telomere shortening, double strand breaks or other DNA lesions caused by oxidative stress. Unfortunately, this phenotype is also defined as a supporter of age-related neurodegeneration (reviewed in Campisi, 2013). In ageing cells the mass of lysosomes is accumulating which results in an increasing activity of the β-galactosidase enzyme. A chemical assay can be used to detect the activity of the senescence-associated ß-galactosidase (SA-β-galactosidase) (Kurz et al., 2000).

Using this assay, no senescence was detectable in WT and mutant NE cells under maintenance conditions (Figure 4.9A). In addition, cells, differentiated for two weeks, were also negative for β-galactosidase activity (Data not shown). In contrast,

cells differentiated for 6 weeks were senescent and exhibited similar amount of SA-ß-gal-positive cells in WT and LRRK2 mutant cells (Figure 4.9B, C).
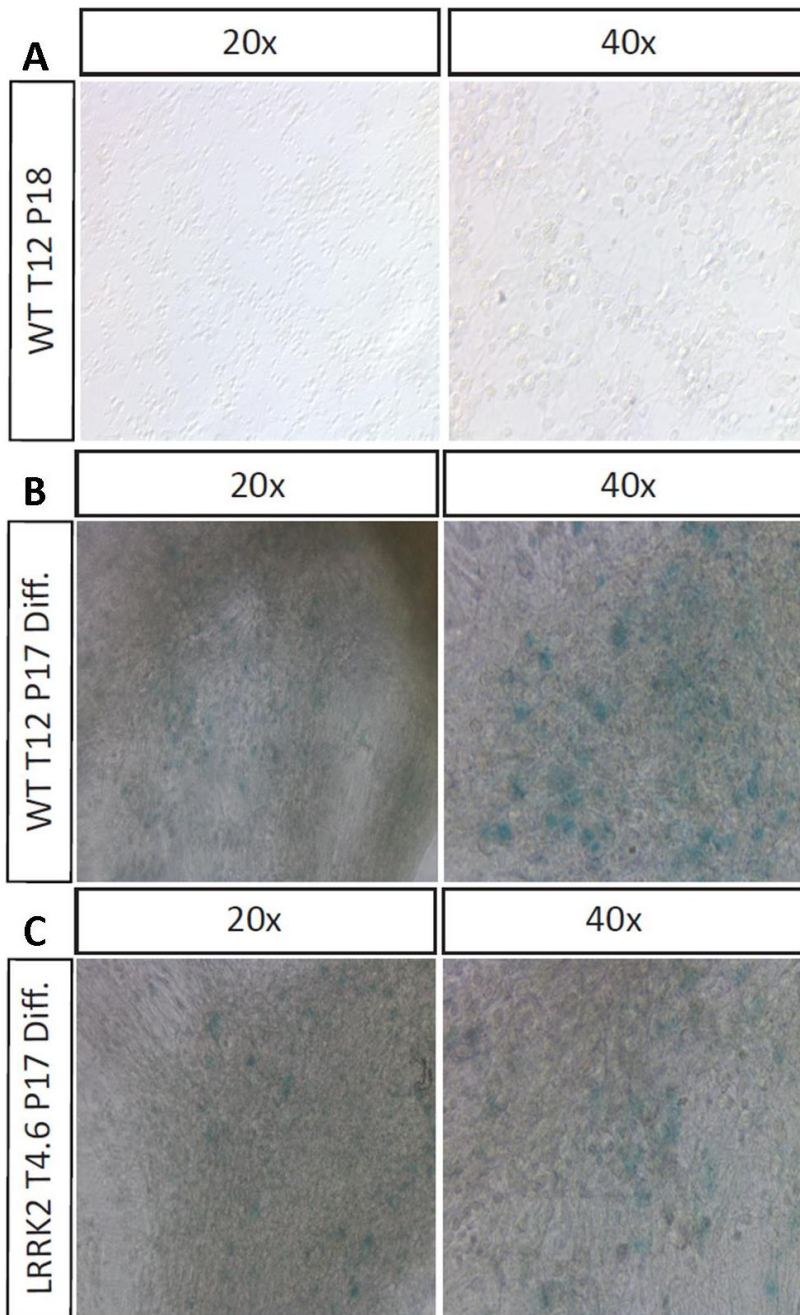

Figure 4.8: Detection of senescent cells. WT and LRRK2 mutant NE cells were seeded on coverslips in a 24-well plate coated with matrigel. **(A)** After two days under maintenance conditions the cells were fixed and the senescence-associated ß-galactosidase staining was performed according to

manufacturer's instructions. In case of the NE cells, no senescence cells were detected as seen in the representative bright field picture. **(B, C)** In colonies of WT and LRRK2 mutant cells that were differentiated for six weeks, senescent cells were detectable (blue dots).

4.2.5 Expression levels of mRNAs

Previous studies revealed the repressing effect of the LRRK2 G2019S mutation on the microRNA let-7a which led to elevated DP1 and E2F1 levels in Drosophila (Gehrke et al., 2010). To determine whether the LRRK2 G2019S mutation has influences on the mRNA levels, a RT-qPCR was carried out using primers to detect mRNAs of common senescence markers (p16, p19, p21), apoptosis activators (p53) and cell cycle regulating proteins (DP1, E2F1). Furthermore, the levels of Ago2 and TRIM32 were assayed to investigate a possible influence of the LRRK2 mutation on their mRNAs levels.

Therefore, mRNA from WT and LRRK2 NE cells was isolated and used as a template for reverse transcription and RT-qPCR. *GAPDH* mRNA was used as a control. Most mRNAs examined, showed similar expression levels in LRRK2 mutant cells compared to WT cells. The only exceptions were *dp1* mRNA with a 4 fold increase in expression levels (not significant), and *e2f1* mRNA which was elevated twofold (Figure 4.10).
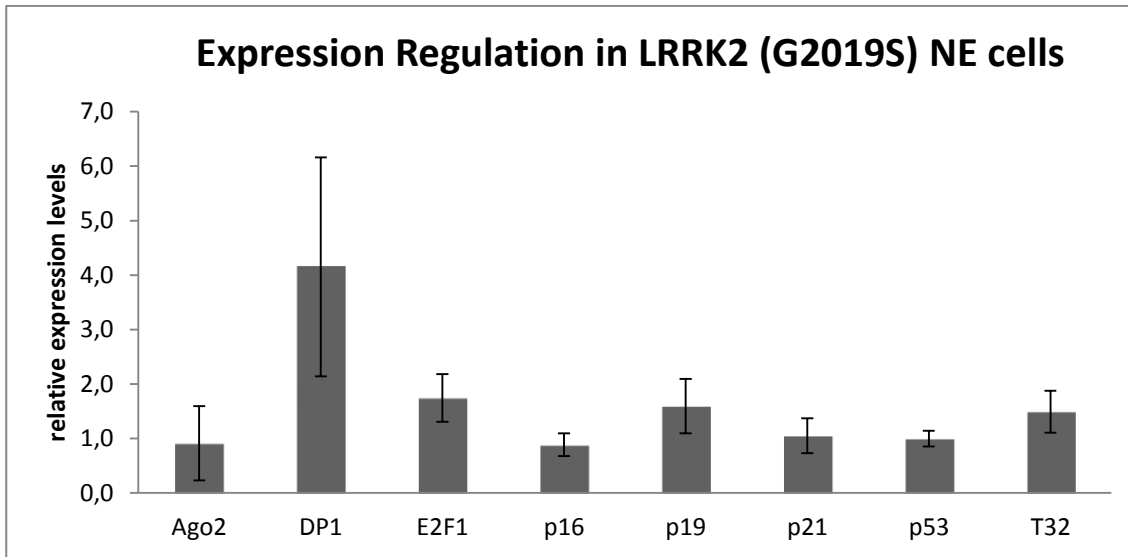
Figure 4.9: mRNA expression levels in LRRK2 mutant NE cells. Quantitative RT-PCR analysis showing relative mRNA expression levels of proteins involved in cell cycle regulation, senecence, apoptosis and differentiation induction. The respective mRNA expression levels in mutant cells were compared to those in WT cells (mean ± s.e.m, n= 3-5).

4.2.6 Subcellular localization of TRIM32 in NE cells

As mentioned before, TRIM32 has been identified to play an important role during neuronal differentiation. Furthermore, studies have shown that TRIM32 is distributed asymmetrically during mitosis of mouse neural progenitor cells and to translocate to the nucleus upon differentiation (Hillje et al., 2011; Schwamborn et al., 2009).

However, it has not been investigated so far, whether this distribution of TRIM32 is conserved in NE cells. To elucidate this question, WT and LRRK2 mutant NE cells of different passages and under maintenance as well as differentiation conditions were stained for TRIM32. As in neural stem cells TRIM32 was localized in the cytoplasm in the multipotent NE cells and was distributed equally between the

cells during mitosis (Figure 4.11). Similarly, during differentiation, TRIM32 translocated into the nucleus and displayed elevated levels (Figure 4.12).
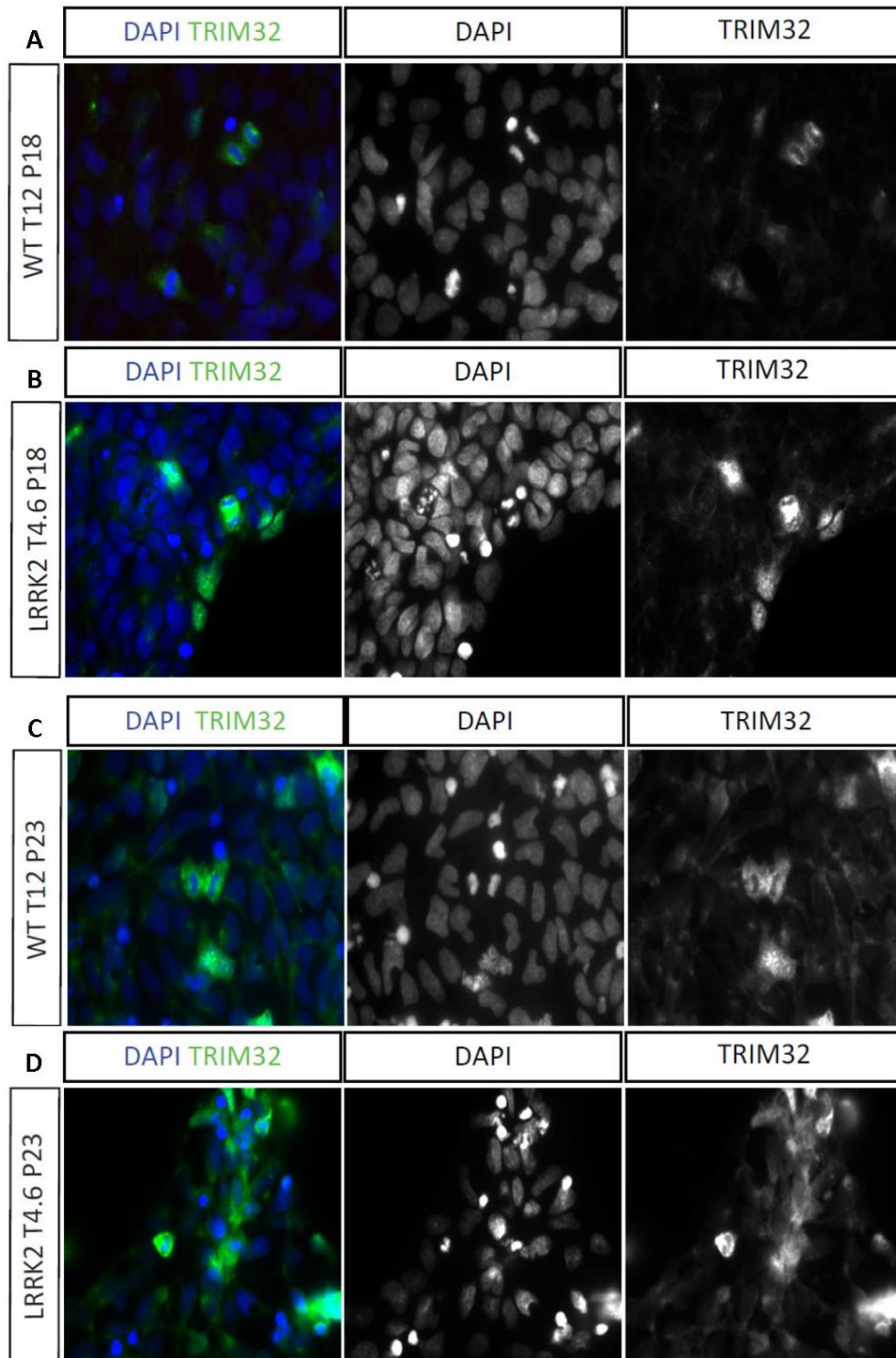
Figure 4.10: Subcellular localization of TRIM32 in different passages of WT and LRRK2 mutant NE cells. NE cultures were cultivated under maintenance conditions on matrigel coated plates. **(A, B)** At p18 and **(C, D)** p23 cells were fixed and stained for TRIM32.
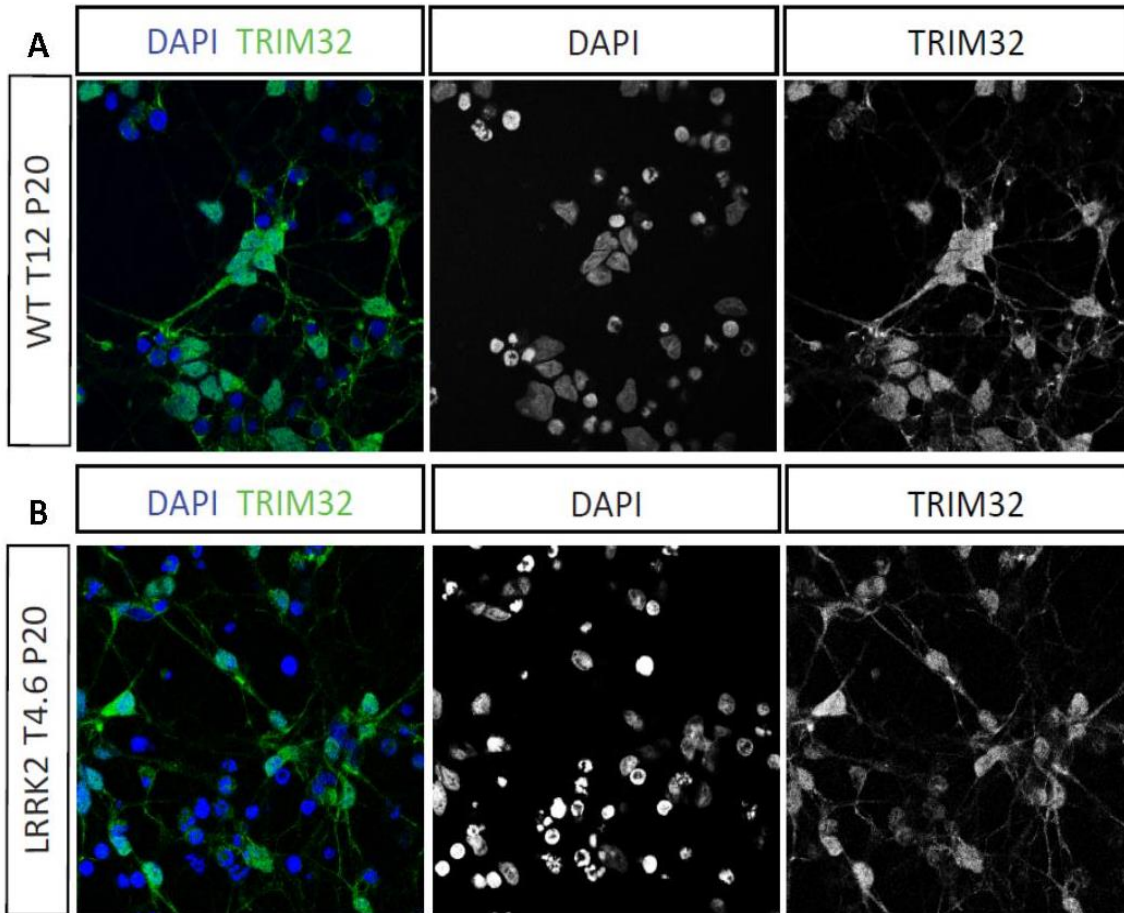

Figure 4.11: TRIM32 localization after differentiation of WT and LRRK2 mutant cells. NE cells were differentiated for 2 weeks with the two step differentiation protocol. **(A, B)** Immunofluorescence pictures were done with the confocal microscope, due to the three dimensional structure of the colonies, to acquire the distribution of the TRIM32 protein in WT and LRRK2 mutant cells at p20.

In summary, the G2019S mutation seems to increase apoptosis and decrease mitophagy rates in proliferating and differentiated NE cells. As an example, the amount of mutant cells undergoing apoptosis was 3 fold higher as in WT cells. In

contrast, regarding the cell cycle neither significant difference under maintenance conditions nor during differentiation was observed.

Furthermore, degradation of dysfunctional mitochondria through lysosomes was decreased in mutant cells, whereas senescence was unaffected. Moreover, the subcellular localization of TRIM32 in dividing and non-dividing cells was not influenced by the LRRK2 mutation.

4.3 Interaction of LRRK2 and TRIM32

LRRK2 and TRIM32 are known to interact with Argonaute proteins and to regulate protein synthesis via the miRNA pathway (Gehrke et al., 2010; Schwamborn et al., 2009). To analyze whether LRRK2 and TRIM32 can interact with each other immunoprecipitation assays (IP) were performed. Therefore, HEK293T cells were co-transfected with plasmids encoding for different FLAG-LRRK2-constructs and HIS-TRIM32. Figure 4.13 displays the western blot of the three different performed IPs. Precipitation of LRRK2 using a α-FLAG antibody revealed the interaction between TRIM32 and the different LRRK2 constructs.
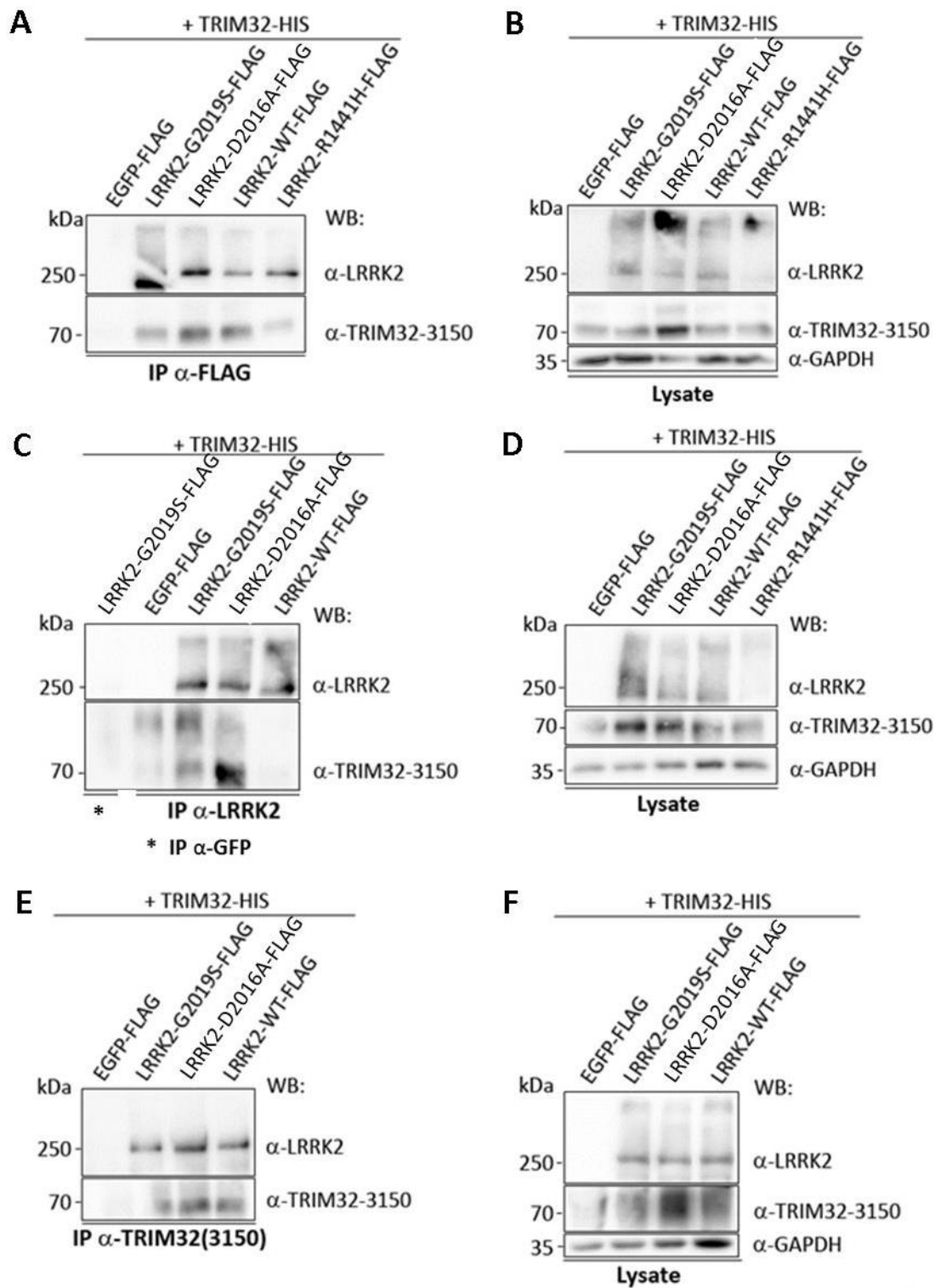
Figure 4.12: Interaction of LRRK2 WT and mutants with TRIM32 in HEK293T cells. HEK293T cells were co-transfected with different FLAG-tagged LRRK2 plasmids and His-tagged TRIM32. 48 h post transfection, the cells were lysed and the lysate was used for an IP. The interaction of LRRK2

and TRIM32 was analyzed using western blots. A control transfection with EGFP-FLAG was done. **(A)** Western blot analysis after IP with α-FLAG antibody and **(B)** of the lysates as a control for protein expression (n=1). **(C)** Western blot analysis after IP with an antibody against LRRK2 and **(D)** of the lysates (n=1). **(E)** Western blot analysis after IP with a TRIM32 antibody and **(F)** of the lysates (n=3). **(B, D, F)** Western blots using an antibody against GAPDH served as a loading control. IP α-GFP antibody = control, WB = Western Blot

In the next step, we investigated whether this interaction is also the case for endogenous proteins in the mouse brains. Since LRRK2 is a very big protein it is difficult to analyze via western blots. Therefore, different cooking times and temperatures were tested to denature the protein. The strongest signal for LRRK2 was obtained after cooking the lysate 1 min at 95 °C. Thus, these conditions were applied to all of the following samples, in which LRRK2 protein levels were analyzed. The band for TRIM32 was detected as a smear due to the short boiling time (Figure 4.14A).

In E13 brain lysates an interaction between LRRK2 and TRIM32 could only be observed after precipitation of LRRK2 but not after precipitation of TRIM32. Interestingly, the endogenous expression levels of both proteins seem to be very low, since no signal was detectable in the lysates for TRIM32 or LRRK2 (Figure 4.14B). In E14 brain lysates TRIM32 could be detected in the lysate, but the IP of TRIM32 was not successful (Figure 4.14C). Moreover, LRRK2 was enriched after IP of both LRRK2 and also TRIM32 although LRRK2 was not detected in the lysate. A faint signal for TRIM32 was detected in the LRRK2 IP.
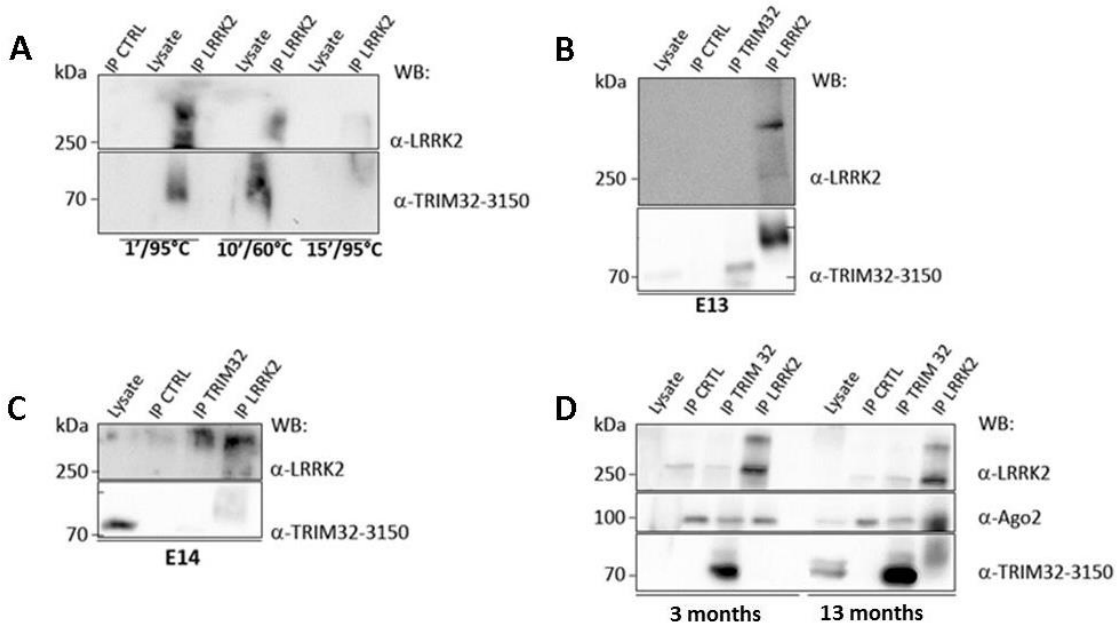
Figure 4.13: Interaction of LRRK2 and TRIM32 at different developmental stages of mouse brains. IPs were performed using a GFP antibody as a control (IP CTRL), a TRIM32 antibody or a LRRK2 antibody. **(A)** Different boiling times and temperatures were tested to obtain better signals for LRRK2. Therefore, IPs from adult mouse brain lysates were performed using a LRRK2 antibody or a GFP antibody as control. The samples were cooked for either 1 min at 95 °C, 10 min at 60 °C or 15 min at 95 °C and analyzed by western blotting. (n=1) **(B)** Western blot analysis of IPs from brain lysates of 5 E13 mouse brains (n=3). **(C)** Western blot analysis of IPs from brain lysates from 5 E14 mice. **(D)** Western blot analysis of IPs from adult brain lysates from 3 month and 13 month old mice (n=5).

The interaction of LRRK2 and TRIM32 was further analyzed in adult brains, which were received from two mice at different ages (Figure 4.14D). Interestingly, the older mouse displayed a strong interaction between the two proteins in comparison to the younger mouse. In the brain lysates of the younger mouse neither LRRK2 nor TRIM32 was detectable indicating only low expression levels. However, precipitation

of LRRK2 and TRIM32 was successful in the young brain but no interaction between the two proteins could be detected (Figure 4.14D).

4.3.1 Effect of ageing on the interaction between LRRK2 and TRIM32

After demonstrating the interaction of endogenous TRIM32 and LRRK2, we were further interested whether the interaction between both proteins changes during development and ageing. Therefore, E13, E18 and E20 mouse brains were used for IPs with antibodies against LRRK2, TRIM32 and GFP as control. Additionally, two adult brains of different ages (5 and 8 months) were used for IPs with the same antibodies. To investigate, whether the interaction between LRRK2 and TRIM32 is dependent on RNA, the IPs from adult brain lysates were also treated with RNAseA.

The protein levels of Ago2 decreased during ageing (Figure 4.15A and B), whereas LRRK2 was absent in embryonic brains and increased during ageing (Figure 4.15A and C). The levels of TRIM32 decreased during embryogenesis and increased again in ageing mice (Figure 4.15A and D).

To analyze possible changes in the interaction of LRRK2 and TRIM32 over time LRRK2 and TRIM32 were precipitated from E13, E18 and E20 lysates. IP of LRRK2 revealed again an interaction with TRIM32 at E18 and E20, but not at E13. Furthermore, with this IP, binding of Ago2 to LRRK2 could be observed. In contrast, although the IP of TRIM32 was successful, only very weak bands for LRRK2 and Ago2 could be detected, that had similar intensity compared to those in the negative control and therefore probably result from unspecific binding (Figure 4.15E). In Figure 4.15F a dependence on RNA of the interaction of LRRK2 and TRIM32 cannot be

observed. Although the IPs with LRRK2 and TRIM32 worked, no interaction was detected.
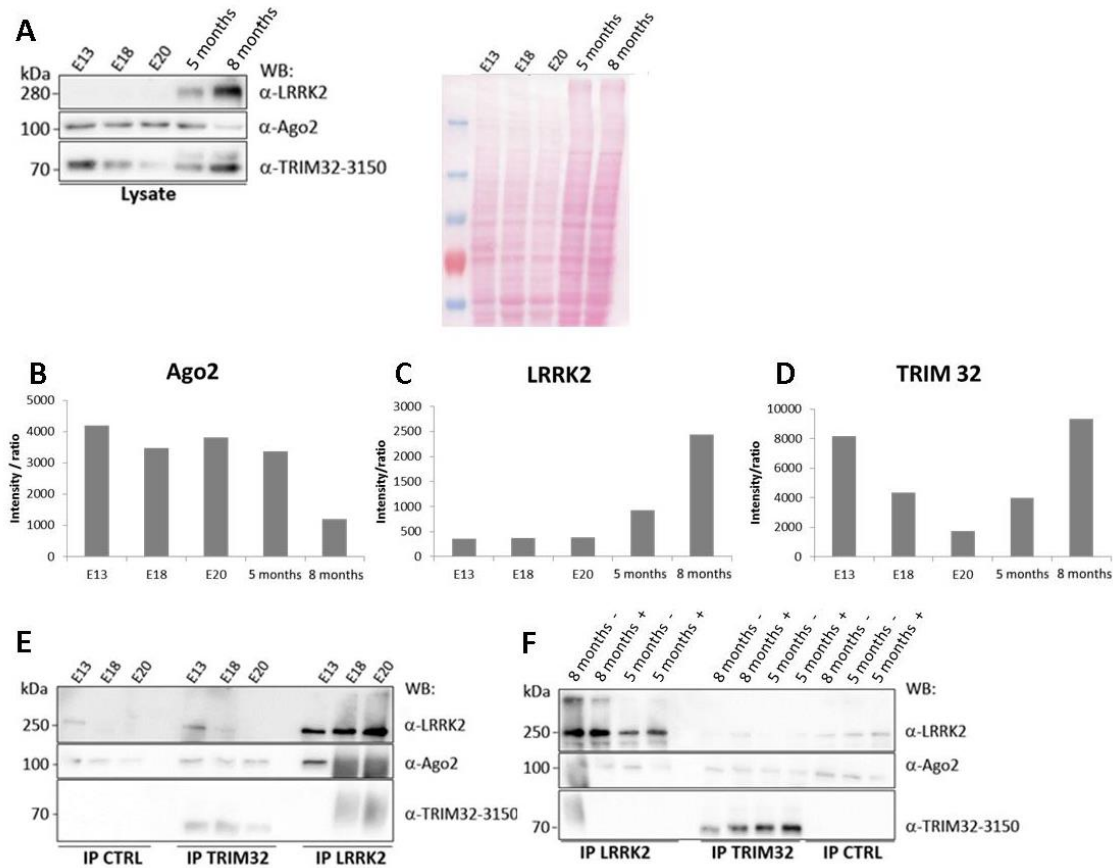

Figure 4.14: Comparison of the interaction between LRRK2 and TRIM32 in embryonic and adult brains as well as in dependence of mRNA. (A) Western blot analysis of the expression levels of LRRK2, Ago2 and TRIM32 at different developmental stages. Ponceau staining of the blot serves as a loading control. **(B-D)** Relative intensities of the protein expression of Ago2, LRRK2 and TRIM32 as shown in **(A)** in comparison to the Ponceau staining. The intensities were measured using ImageJ and calculated with Microsoft Excel. **(E)** Western blot analysis of LRRK2, Ago2 and TRIM32 after IP of LRRK2 and TRIM32 from E13, E18 and E20 brains lysates. An IP with a GFP antibody was used as a control (n=2). **(F)** Western blot analysis of LRRK2, Ago2 and TRIM32 after IP of LRRK2 and TRIM32. The IP samples were treated with (+) or without (-) 2 µl RNAse A to investigate the mRNA dependence of the interactions (n=2).

4.3.2 mRNAs and miRNAs bound by the complex

As described earlier, the homologue of TRIM32 (Brat) and LRRK2 in Drosophila were verified to interact with Ago1. Furthermore, it has been described that LRRK2 is able to relieve the suppressive influence of let-7 and miR-184* on *dp1* and *e2f1* mRNA levels (Gehrke et al., 2010). Since let-7a was also shown to be a downstream target of TRIM32 (Schwamborn et al., 2009) we aimed to investigate whether let-7a, miR-184, *dp1* or *e2f1* are also enriched in the LRRK2–TRIM32 complex.

Therefore, LRRK2 and TRIM32 were precipitated from mouse brains at different developmental stages. Subsequently, the beads were utilized for reverse transcription of the precipitated mRNAs and miRNAs into cDNA, which was subjected to RT-qPCR. Primers for miR-184* were not available, so we decided to use the primers for miR-184.

This experiment revealed that all mRNAs and miRNAs of interest were present in the LRRK2-/TRIM32-complexes with changing levels during development (Figure 4.16). The levels of miRNAs as well as mRNA were differently enriched in the complexes of LRRK2 and TRIM32. The opposite enrichments of the complexes with miRNAs and mRNAs could lead to the suggestion of an opposite effects of TRIM32 and LRRK2 on the cell fate. Nevertheless, these data have to be further verified again.
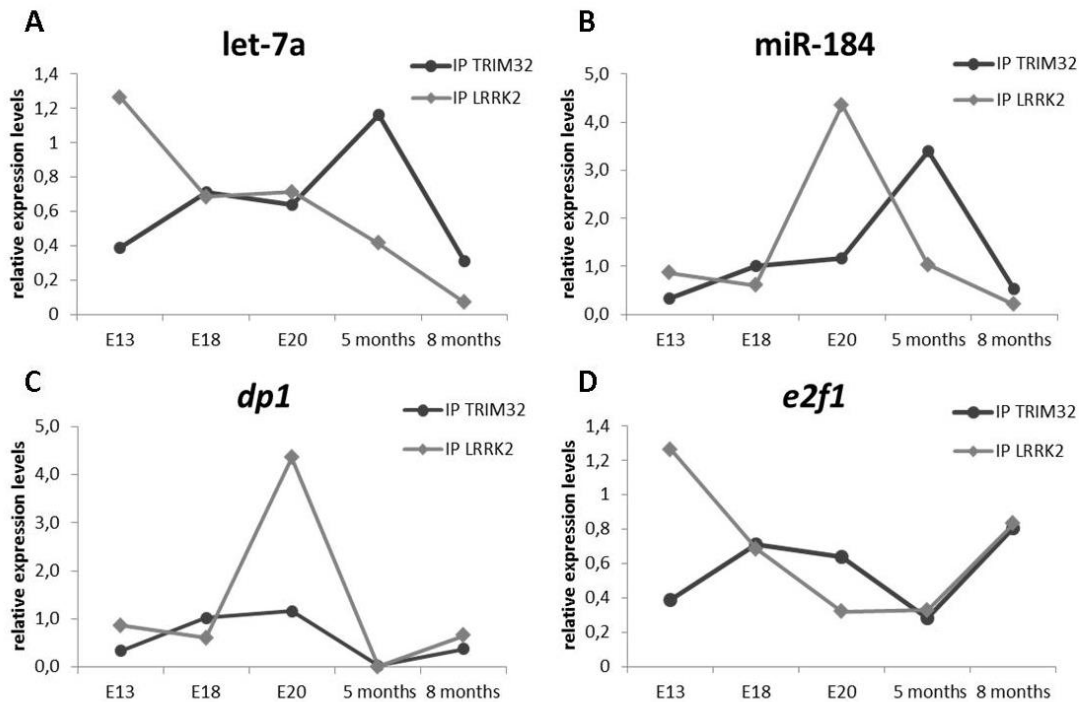
Figure 4.15: miRNAs and mRNAs present in TRIM32- or LRRK2-IPs during aging. Brains lysates of E13, E18 and E20 mice and adult mice were used for IPs with LRRK2 and TRIM32 antibodies. A fraction of the beads was taken for reverse transcription to generate cDNA for the RT-qPCR. **(A-D)** RT-qPCR data showing the levels of bound miRNAs let-7a, miR-184 and mRNAs *dp1*, *e2f1* after IP of TRIM32 or LRRK2, respectively, in comparison to a control IP using a GFP antibody (E13, E18 and E20 n=2; adults n=1).

In conclusion, these results demonstrate that LRRK2 and TRIM32 interact with each other in HEK293T cells as well as in mouse brains at the endogenous protein levels. However, it remains to be analyzed whether this interaction is direct or dependent on RNA. Furthermore, it could be shown that Ago2, LRRK2 and TRIM32 exhibit an age-dependent expression pattern. Finally, the LRRK2- and TRIM32-complexes were shown to contain miRNAs as let-7a and miR-184 as well as *dp1* and *e2f1* mRNAs with changing levels depending on the developmental stage and age of the mice.

5 Discussion

The results presented in this thesis demonstrate the differentiation ability of NE cells as early neural progenitors and the effects of the G2019S mutation on the viability of these cells. The LRRK2 mutation G2019S leads to progressive apoptosis in proliferating as well as differentiated NE cells, which was three fold higher compared to WT cells. Moreover, the G2019S mutation decreases recycling of damaged mitochondria through mitophagy. Although the LRRK2 mutation has no influence on the distribution on TRIM32 in proliferating NE cells or during differentiation, an interaction of LRRK2 and TRIM32 on exogenous as well as endogenous levels could be shown. Furthermore, an age-dependent correlation of the expression levels of Ago2, LRRK2 and TRIM32 was found. This was also the case for the miRNAs and mRNAs let7a, miR-184, *e2f1* and *dp1*, which co-precipitated with LRRK2 and TRIM32 and displayed altered expression levels at different development stages and during ageing. This leads to the conclusion that LRRK2 and TRIM32 may play an important role in regulating the balance between proliferation and differentiation in NE cells.

5.1 Differentiation potential of NE cells

Previous studies have demonstrated the ability of NE cells to form neural rosettes (Reinhardt et. al., 2013). This capability could be further supported in this thesis by adding FGF2 to NE cells leading to their differentiation into neural rosettes. Moreover, a translocation of TRIM32 into the nucleus was observed in NE cells upon differentiation, already at early developmental stages. This is consistent with other

studies showing the nuclear translocation of TRIM32 in differentiating NSCs (Hillje et al., 2011; Schwamborn et al., 2009)

In order to gain more insights into the influence of TRIM32 on neural development of NE cells, it may be useful to differentiate the neural rosettes further into neurons and examine the localization of TRIM32 all along this process. Additionally, differentiation of NE cells bearing the G2019S mutation into rosettes and further into neurons could indicate whether the mutation influences the differentiation abilities of stem cells in early or rather late stages.

5.2 Impacts of the LRRK2 G2019S mutation

The toxic effect of G2019S has already been shown for human neuroblastoma cells (SH-SY5Y) and primary neurons (Smith et al., 2006). Additionally, experiments in transgenic mice revealed a reduced proliferation rate in cells bearing the G2019S mutation (Winner et al., 2011). On the other hand, the absence of LRRK2 in human mesencephalic neural progenitor cells (hmNPCs) was shown to result in a reduced capacity to differentiate into dopaminergic neurons. Interestingly, the proliferation marker Ki67 was found to be expressed in dying dopaminergic neurons, which point out a re-entry into cell cycle of the neurons (Milosevic et al., 2009). However, the influence of the G2019S mutation has not been investigated at an early stage of neural stem cell differentiation so far.

To address this question, we sought for differences in proliferation and apoptosis between WT and mutated NE cells. The G2019S LRRK2 mutation led to a threefold increase in the amount of apoptotic NE cells as has been shown for hmNPCs and neuroblastoma cells (Milosevic et al., 2009; Smith et al., 2006). In

contrast, no significant differences in the expression levels of proliferation markers were observed at the multipotent cell stage. However, in later passages WT cells displayed a higher expression of PH3 positive cells compared to mutant cells, while the amount of apoptotic cells increased in both cases.

Studies have examined during long-term cultivation of differentiated neurons that neurons carrying the G2019S mutation revealed less neurites and simpler processes compared to healthy neurons. In addition, these cells underwent apoptosis more frequently (Sánchez-Danés et al., 2012). We sought at two different time points of differentiation for differences in apoptosis rates of WT and NE cells bearing the G2019S mutation. The amount of apoptotic cells increased in both cases during differentiation but remained accelerated in mutant cells.

Considering the cell cycle stainings, further experiments have to be done to approve whether the value of 4 % for cells in proliferation is correct. In contrast, during test stainings (not shown) the cells exhibited a proliferation rate around 25 %. Furthermore, despite an elevated apoptosis rate in the mutant culture, both cell lines reached confluency at the same time. This reveals a conflict in the cell cycle staining experiments which has to be further verified. Additional stainings for cell cycle markers at lower cell densities and over a longer time of passages may display whether there is a decline in proliferation during ageing of the mutant NE cells.

The mechanism how the mutation causes progressive apoptosis is currently unknown. Our results confirmed recent observations and indicate that neural epithelial cells are already affected by the G2019S mutation *in vitro*. However, patients carrying the G2019S LRRK2 mutation usually develop Parkinson's disease not before an age of 50 years. The accelerated proliferation rate of affected cells at

early stages may be sufficient to avoid an earlier advance of the disease. In this way, a balance between dying and generation of new neurons is achieved at least in the younger days. The effect of ageing on the NE cells bearing the G2019S mutation has to be further investigated.

5.2.1 Impairment of autophagy

Recent studies revealed that LRRK2 is localized to the cytoplasm and associated to the outer membrane of mitochondria (West et al., 2005). Like Parkin or Pink1, LRRK2 plays an important role in clearing of dysfunctional mitochondria and within the autosomal-lysosomal pathway. It has been shown, that in the kidneys of mice a dramatic accumulation and aggregation of α-synuclein and ubiquitinylated proteins is caused by reduced autophagy activity due to the absence of LRRK2. In contrast, in the mouse brain LRRK1 is suggested to play a compensatory role (Tong et al., 2010).

We were interested whether an increased kinase activity caused by the G2019S mutation of LRRK2 results in a similar phenotype. The effect of mitophagy was significantly reduced in cells bearing the mutation. However, differentiation of the NE cells led to an increase of co-localization of mitochondria and lysosomes, which was still reduced compared to WT cells. Thus, our results confirm the impairment of the autophagy pathway in NE cells carrying the G2019S mutation.

Interestingly, we could observe a change in the staining pattern of mitochondria which has not been reported so far. In multipotent NE cells the mitochondria were distributed equally throughout the cytoplasm whereas in

differentiated cells they displayed a more punctuated pattern. This may result from the accumulation of dysfunctional mitochondria due to their impaired degradation.

5.2.2 Influence of G2019S LRRK2 on senescence.

Senescence as well as apoptosis increases during ageing. Therefore, we were interested whether the G2019S mutation has any influence on the occurrence of senescence. As suggested, no senescent cells were observed in any of the NE cultures. Furthermore, the results showed neither an increase in senescence nor a higher density of senescent cells in the compared colonies of WT or LRRK2 mutated differentiated cells.

  These results suggest that the G2019S mutation has no impact on the development of senescence. However, it could also be the case, that, due to the increased apoptosis rate, cells with the G2019S mutation die before reaching a senescent state. Nevertheless, further studies in long-term differentiated cultures of G2019S need to be done to verify this hypothesis.

5.3 Affected mRNA levels

Besides the expression levels of cell cycle or senescence markers, the mRNA expression levels of other cell cycle regulating genes were analyzed. We observed a highly fluctuating expression pattern of all chosen mRNAs. Thus, this experiment has to be repeated to confirm these results. *Dp1* and *e2f1* seem to be elevated in LRRK2 compared to WT brains. These mRNAs have been found to be influence by LRRK2

expression before and also showed an increase in the presence of the G2019S mutation (Gehrke et al., 2010b).

In the same study, an interaction between LRRK2 and Ago2 was examined. Moreover, another study revealed an interaction between TRIM32 and Ago1 (Schwamborn et al., 2009). To this end, Ago2 and TRIM32 mRNA expression levels were also increased in our experiment. Thus, lead to the hypothesis that a complex with all three proteins exist which regulations miRNA repression.

The influence of the LRRK2 G2019S mutation on the mRNAs expression levels of *p16*, *p19*, *p21* and *p53* is just marginally. Nevertheless, all of those proteins are described to have influence on neural differentiation (Bruggeman and Van Lohuizen, 2006). Especially the p19-p53 pathway has been found to repress Myc and to attenuate cell cycle progression (Nagao et al., 2008). Accordingly, LRRK2 may also have an effect on this pathway due to its function in differentiation of dopaminergic neurons and cell death (Milosevic et al., 2009). However, since all of the mRNAs analyzed showed a highly fluctuating expression pattern within the different experiments, these experiments have to be repeated to confirm the results. Nevertheless, these data indicate that the LRRK2 G2019S mutation negatively regulates the expression of certain mRNAs.

Possible reasons for the high levels of fluctuations may be that the density of the cells was not taken into account, which can have a high impact on the expression levels of cell cycle markers. Therefore, for future experiments, it is recommendable to seed the same amount of cells for each cell line. Additionally, it would be interesting to analyze the mRNA levels over time to see whether they are also age-dependently regulated.

5.4 Localization of TRIM32

TRIM32 is known to play an important role during neuronal differentiation. It is distributed asymmetrically during mitosis of mouse neural stem cells and the cell that inherits the TRIM32 protein differentiates into a neuron while the cell with low levels of TRIM32 remains in a neural stem cell fate. (Hillje et al., 2011; Schwamborn et al., 2009).

As described for NSCs, a nuclear translocation of TRIM32 was observed in NE cells upon differentiation. Interestingly, no difference was observed in the distribution of TRIM32 in WT and mutant NE cells, indicating that the G2019S mutation has no influence on the localization of TRIM32.

5.5 Interaction of LRRK2 and TRIM32 during development

It is known that TRIM32 and LRRK2 function in an opposite manner on the RNAi silencing system. For instance, it has been shown that pathogenic LRRK2 can bind to Ago1 and represses the inhibition of the mRNAs *e2f1* and *dp1* through the miRNAs let7 and miR-184* (Gehrke et al., 2010). On the other hand, TRIM32 has been reported to activate the c-Myc repression via let-7a (Schwamborn et al., 2009).

Therefore, we wanted to investigate whether LRRK2 and TRIM32 can directly interact with each other. Via Immunoprecipitation experiments, the interaction between LRRK2 and TRIM32 could be demonstrated on the exogenous as well as endogenous protein levels. Interestingly, when investigating the interactions of the exogenous proteins in HEK293T cells, the overexpressed LRRK2-FLAG constructs could never be detected via their FLAG-tags in any approach. An insufficient transfection or inaccessibility of the tag due to protein structures can be determining

factors for the unsuccessful Flag-tag detection. Furthermore, LRRK2 is a large protein and hence troubles to detect in western blots (Biskup et al., 2007). However, detection of LRRK2 was possible using a LRRK2 antibody. Regarding the different LRRK2 constructs, it appeared that some mutant LRRK2 constructs interacted stronger with TRIM32 than the WT protein, as for example the kinase dead mutant D2016A.

The interaction of endogenous LRRK2 and TRIM32 was observed at different stages of development in the mouse brain. Interestingly, the interaction seems to be weaker at the early developmental stages compared to the adult one. The protein levels of LRRK2 and TRIM32 deviates and due to these changes the interaction may adapt. LRRK2, for example is suggested to be low expressed during embryogenesis whereas it is found in increased levels after development. In comparison, TRIM32 can be detected with increasing amounts during development.

A caveat to this study is that the interaction of LRRK2 and TRIM32 was mainly shown after co-precipitating TRIM32 with LRRK2 but not the other way around. A reason could be that LRRK2 binds another protein which interacts with TRIM32 and leads to a pull down of TRIM32. Another explanation may be the different boiling times. The samples of the TRIM32 IP were boiled for 15 min, which is probably too long to detect LRRK2. As also observed in the test of different boiling times, where a signal for LRRK2 could only be detected after 1 or 10 min boiling time, but not after 15 min. Thus, in future experiments, the boiling time of the TRIM32 IP samples should be decreased.

LRRK2 is expressed from E17 on and throughout post-natal development in whole mouse brain lysates (Biskup et al., 2007). However, we could LRRK2 only

detect in minor levels until E20. In the brains of 3 and 8 month old mice the expression of LRRK2 was increasing. In contrast, the levels of Ago2 reached the lowest point in the 8 month brain. TRIM32 levels were detected in high amounts in the E13 and 8 month brain and during development it decreased with the lowest expression around E20 afterwards it increased again. Nevertheless, these changes in expression levels may correlate with the development of the brain. During the E13 and E20 stages the cells are differentiating and migrating and therefore Ago2 and TRIM32 are highly expressed. LRRK2 was described for inhibition of differentiation; therefore, it is marginally expressed during development. Moreover, the increased expression level of the 8 month brain may correlate with a raise of *e2f1* and *dp1* expression.

Furthermore, treatment of the IP samples with RNAse did not exhibit a significant effect on the precipitation of the LRRK2-TRIM32 complex. In conclusion, the interaction of LRRK2 and TRIM32 is independent of the presence of RNA. To evaluate whether LRRK2 and TRIM32 compete for binding to Ago2, further analysis, with for example different concentrations of the proteins, have to be done

5.6 miRNAs and mRNAs present in the complexes

The interplay between TRIM32 and different miRNAs as for example let-7a has already been shown as well as the influence of LRRK2 on the expression levels of e*2f1* and dp*1* via its inhibition of let-7a (Gehrke et al., 2010b) (Schwamborn et al., 2009). Consequently, we aimed to investigate whether these miRNAs and mRNAs are included in the LRRK2-TRIM32 complexes. Interestingly, the RT-qPCRs after IP

revealed that LRRK2 and TRIM32 seem to have antagonizing binding affinities to the chosen targets at different stages of brain development.

So far only miR-184* has been shown to interact with LRRK2 and to repress the expression of *e2f1* (Gehrke et al., 2010b). We could not acquire a primer pair for miR-184* so we switched to miR-184 and examined for a possible interaction. Our results demonstrate the presence of miR-184 within the LRRK2-TRIM32 complex. According to the qPCR data, the amount of miR-184 bound by the complex negatively correlates to the amount of let-7a. This is consistent to what is known from the literature, because let-7a and TRIM32 have been described to induce differentiation whereas LRRK2 and miR-184 inhibit differentiation and favor proliferation (Gehrke et al., 2010b; Schwamborn et al., 2009). The results displayed in figure 4.16 suggest that during the development between E13 and E18, let-7a as well as miR-184 keep a balance between proliferation and differentiation in the mouse brain. In contrast, at E20 miR-184 exhibited a peak which may correlate with an increase in proliferation followed by elevated differentiation. This may be due to the development of the rods and initial differentiation of layer V the internal pyramidal layer in the mammalian brain at this stage (Finlay and Darlington, 1995). The expression levels from the old adult mouse brains confirm the suggestion that differentiation and proliferation of the cells decrease during ageing.

Expression levels of the mRNAs for *e2f1* and *dp1* were also found to be present in the LRRK2-TRIM32 complexes. The interaction between E2F1 and DP1 is necessary for cell cycle progression (Ishida et al., 2005). Interestingly, the levels of *e2f1* decreased from post-natal day 10 to 3 months in mice which suggest, that the proliferation rates in at this time are somehow diminished. However, other studies

showed that overexpression of E2F1 and its dimerization partner DP1 leads to programmed cell death in *Drosophila* (Brennecke et al., 2003). The RT-qPCR data implicate that LRRK2 interacts stronger with the mRNAs of *dp1* and *e2f1* in comparison to TRIM32. The peak of *dp1* in E20 correlates with the peak of miR-184 and suggests an increase in proliferation although the mRNA levels of *e2f1* in the LRRK2 IP are at its lowest point. This may be due to a higher translation rate of the *e2f1* mRNA. In contrast, both expression levels of *e2f1* and *dp1* correlate in adult mouse brains. An increase in the oldest brain (8 months) suggests again an increase of proliferation which could also lead to programmed cell death. In contrast, an increase in these mRNAs could be due to an extended cell cycle of adult neural stem cells in higher aged brain. For instance, the role of E2F1 in neurodegeneration has been shown in Parkinson's disease models and an activated pRB/E2F pathway has been found in dopaminergic neurons. Despite reactivating proliferation, E2F1 led to cell death of the dopaminergic neurons (Höglinger et al., 2007).

To investigate the role of LRRK2 and TRIM32 in cell cycle and apoptosis pathways more precisely, different regions like the subventricular zone have to be examined separately. The heterogeneity of the mouse brain can influence the RT-qPCR results and lead to high variability. Therefore, the results have to be further verified in different parts of the brain.

6 References

Abou-Sleiman, P.M., Healy, D.G., Wood, N.W., 2004. Causes of Parkinson's disease: genetics of DJ-1. Cell Tissue Res. 318, 185–188.

Bartel, D.P., 2004. MicroRNAs: genomics, biogenesis, mechanism, and function. Cell 116, 281–297.

Biskup, S., Moore, D.J., Rea, A., Lorenz-Deperieux, B., Coombes, C.E., Dawson, V.L., Dawson, T.M., West, A.B., 2007. Dynamic and redundant regulation of LRRK2 and LRRK1 expression. BMC Neuroscience 8, 102.

Bolte, S., Cordelières, F.P., 2006. A guided tour into subcellular colocalization analysis in light microscopy. J Microsc 224, 213–232.

Braak, H., Del Tredici, K., Rüb, U., De Vos, R.A.I., Jansen Steur, E.N.H., Braak, E., 2003. Staging of brain pathology related to sporadic Parkinson's disease. Neurobiol. Aging 24, 197–211.

Braak, H., Ghebremedhin, E., Rüb, U., Bratzke, H., Del Tredici, K., 2004. Stages in the development of Parkinson's disease-related pathology. Cell Tissue Res. 318, 121–134.

Brennecke, J., Hipfner, D.R., Stark, A., Russell, R.B., Cohen, S.M., 2003. bantam encodes a developmentally regulated microRNA that controls cell proliferation and regulates the proapoptotic gene hid in Drosophila. Cell 113, 25–36.

Bruggeman, S.W.M., Van Lohuizen, M., 2006. Controlling stem cell proliferation: CKIs at work. Cell Cycle 5, 1281–1285.

Campisi, J., 2013. Aging, Cellular Senescence, and Cancer. Annual Review of Physiology 75, 685–705.

Chiang, A.P., Beck, J.S., Yen, H.-J., Tayeh, M.K., Scheetz, T.E., Swiderski, R.E., Nishimura, D.Y., Braun, T.A., Kim, K.-Y.A., Huang, J., Elbedour, K., Carmi, R., Slusarski, D.C., Casavant, T.L., Stone, E.M., Sheffield, V.C., 2006. Homozygosity mapping with SNP arrays identifies TRIM32, an E3 ubiquitin ligase, as a Bardet-Biedl syndrome gene (BBS11). Proc. Natl. Acad. Sci. U.S.A. 103, 6287–6292.

Choi, J., Levey, A.I., Weintraub, S.T., Rees, H.D., Gearing, M., Chin, L.-S., Li, L., 2004. Oxidative modifications and down-regulation of ubiquitin carboxyl-terminal hydrolase L1 associated with idiopathic Parkinson's and Alzheimer's diseases. J. Biol. Chem. 279, 13256–13264.

Cookson, M.R., 2010. The role of leucine-rich repeat kinase 2 (LRRK2) in Parkinson's disease. Nat. Rev. Neurosci. 11, 791–797.

Cuervo, A.M., Stefanis, L., Fredenburg, R., Lansbury, P.T., Sulzer, D., 2004. Impaired degradation of mutant alpha-synuclein by chaperone-mediated autophagy. Science 305, 1292–1295.

Doe, C.Q., 2008. Neural stem cells: balancing self-renewal with differentiation. Development 135, 1575–1587.

Duan, X., Kang, E., Liu, C.Y., Ming, G., Song, H., 2008. Development of neural stem cell in the adult brain. Current Opinion in Neurobiology 18, 108–115.

Elkabetz, Y., Panagiotakos, G., Al Shamy, G., Socci, N.D., Tabar, V., Studer, L., 2008. Human ES cell-derived neural rosettes reveal a functionally distinct early neural stem cell stage. Genes Dev. 22, 152–165.

Encinas, J.M., Michurina, T.V., Peunova, N., Park, J.-H., Tordo, J., Peterson, D.A., Fishell, G., Koulakov, A., Enikolopov, G., 2011. Division-coupled astrocytic differentiation and age-related depletion of neural stem cells in the adult hippocampus. Cell Stem Cell 8, 566–579.

Ferraris, A., Ialongo, T., Passali, G.C., Pellecchia, M.T., Brusa, L., Laruffa, M., Guidubaldi, A., Paludetti, G., Albanese, A., Barone, P., Dallapiccola, B., Valente, E.M., Bentivoglio, A.R., 2009. Olfactory dysfunction in Parkinsonism caused by PINK1 mutations. Movement Disorders 24, 2350–2357.

Finlay, B.L., Darlington, R.B., 1995. Linked regularities in the development and evolution of mammalian brains. Science 268, 1578–1584.

Frosk, P., Weiler, T., Nylen, E., Sudha, T., Greenberg, C.R., Morgan, K., Fujiwara, T.M., Wrogemann, K., 2002. Limb-girdle muscular dystrophy type 2H associated with mutation in TRIM32, a putative E3-ubiquitin-ligase gene. Am. J. Hum. Genet. 70, 663–672.

Gage, F.H., 1998. Discussion point Stem cells of the central nervous system. Current Opinion in Neurobiology 8, 671–676.

Galter, D., Westerlund, M., Carmine, A., Lindqvist, E., Sydow, O., Olson, L., 2006. LRRK2 expression linked to dopamine-innervated areas. Ann. Neurol. 59, 714–719.

Gehrke, S., Imai, Y., Sokol, N., Lu, B., 2010a. Pathogenic LRRK2 negatively regulates microRNA-mediated translational repression. Nature 466, 637–641.

Greggio, E., Cookson, M.R., 2009. Leucine-rich repeat kinase 2 mutations and Parkinson's disease: three questions. ASN Neuro 1.

Halliday, G.M., McCann, H., 2010. The progression of pathology in Parkinson's disease. Annals of the New York Academy of Sciences 1184, 188–195.

Han, X., Du, H., Massiah, M.A., 2011. Detection and characterization of the in vitro e3 ligase activity of the human MID1 protein. J. Mol. Biol. 407, 505–520.

Hattiangady, B., Shetty, A.K., 2008. Aging does not alter the number or phenotype of putative stem/progenitor cells in the neurogenic region of the hippocampus. Neurobiol. Aging 29, 129–147.

Hillje, A.-L., Worlitzer, M.M.A., Palm, T., Schwamborn, J.C., 2011. Neural stem cells maintain their stemness through protein kinase C ζ-mediated inhibition of TRIM32. Stem Cells 29, 1437–1447.

Höglinger, G.U., Breunig, J.J., Depboylu, C., Rouaux, C., Michel, P.P., Alvarez-Fischer, D., Boutillier, A.-L., Degregori, J., Oertel, W.H., Rakic, P., Hirsch, E.C., Hunot, S., 2007. The pRb/E2F cell-cycle pathway mediates cell death in Parkinson's disease. Proc. Natl. Acad. Sci. U.S.A. 104, 3585–3590.

Höglinger, G.U., Rizk, P., Muriel, M.P., Duyckaerts, C., Oertel, W.H., Caille, I., Hirsch, E.C., 2004. Dopamine depletion impairs precursor cell proliferation in Parkinson disease. Nat. Neurosci. 7, 726–735.

Ishida, H., Masuhiro, Y., Fukushima, A., Argueta, J.G.M., Yamaguchi, N., Shiota, S., Hanazawa, S., 2005. Identification and characterization of novel isoforms of human DP-1: DP-1{alpha} regulates the transcriptional activity of E2F1 as well as cell cycle progression in a dominant-negative manner. J. Biol. Chem. 280, 24642–24648.

Johnson, C.D., Esquela-Kerscher, A., Stefani, G., Byrom, M., Kelnar, K., Ovcharenko, D., Wilson, M., Wang, X., Shelton, J., Shingara, J., Chin, L., Brown, D., Slack, F.J., 2007. The let-7 microRNA represses cell proliferation pathways in human cells. Cancer Res. 67, 7713–7722.

Jorgensen, N.D., Peng, Y., Ho, C.C.-Y., Rideout, H.J., Petrey, D., Liu, P., Dauer, W.T., 2009. The WD40 domain is required for LRRK2 neurotoxicity. PLoS ONE 4, e8463.

Kahle, P.J., Neumann, M., Ozmen, L., Muller, V., Jacobsen, H., Schindzielorz, A., Okochi, M., Leimer, U., Van Der Putten, H., Probst, A., Kremmer, E., Kretzschmar, H.A., Haass, C., 2000. Subcellular localization of wild-type and Parkinson's disease-associated mutant alpha -synuclein in human and transgenic mouse brain. J. Neurosci. 20, 6365–6373.

Kroemer, G., Mariño, G., Levine, B., 2010. Autophagy and the integrated stress response. Mol Cell 40, 280–293.

Kudryashova, E., Wu, J., Havton, L.A., Spencer, M.J., 2009. Deficiency of the E3 ubiquitin ligase TRIM32 in mice leads to a myopathy with a neurogenic component. Hum. Mol. Genet. 18, 1353–1367.

Kurz, D.J., Decary, S., Hong, Y., Erusalimsky, J.D., 2000. Senescence-associated (beta)-galactosidase reflects an increase in lysosomal mass during replicative ageing of human endothelial cells. J. Cell. Sci. 113 (Pt 20), 3613–3622.

Lipinski, M.M., Zheng, B., Lu, T., Yan, Z., Py, B.F., Ng, A., Xavier, R.J., Li, C., Yankner, B.A., Scherzer, C.R., Yuan, J., 2010. Genome-wide analysis reveals mechanisms modulating autophagy in normal brain aging and in Alzheimer's disease. Proc. Natl. Acad. Sci. U.S.A. 107, 14164–14169.

Locke, M., Tinsley, C.L., Benson, M.A., Blake, D.J., 2009. TRIM32 is an E3 ubiquitin ligase for dysbindin. Hum Mol Genet 18, 2344–2358.

Lois, C., Alvarez-Buylla, A., 1994. Long-distance neuronal migration in the adult mammalian brain. Science 264, 1145–1148.

Lu, Y.W., Tan, E.-K., 2008. Molecular biology changes associated with LRRK2 mutations in Parkinson's disease. J. Neurosci. Res. 86, 1895–1901.

Lugert, S., Basak, O., Knuckles, P., Haussler, U., Fabel, K., Götz, M., Haas, C.A., Kempermann, G., Taylor, V., Giachino, C., 2010. Quiescent and active hippocampal neural stem cells with distinct morphologies respond selectively to physiological and pathological stimuli and aging. Cell Stem Cell 6, 445–456.

Mata, I.F., Wedemeyer, W.J., Farrer, M.J., Taylor, J.P., Gallo, K.A., 2006. LRRK2 in Parkinson's disease: protein domains and functional insights. Trends Neurosci. 29, 286–293.

Milosevic, J., Schwarz, S.C., Ogunlade, V., Meyer, A.K., Storch, A., Schwarz, J., 2009. Emerging role of LRRK2 in human neural progenitor cell cycle progression, survival and differentiation. Mol Neurodegener 4, 25.

Ming, G., Song, H., 2005. Adult Neurogenesis in the Mammalian Central Nervous System. Annual Review of Neuroscience 28, 223–250.

Mouradian, M.M., 2012. MicroRNAs in Parkinson's disease. Neurobiol. Dis. 46, 279–284.

Nagao, M., Campbell, K., Burns, K., Kuan, C.-Y., Trumpp, A., Nakafuku, M., 2008. Coordinated control of self-renewal and differentiation of neural stem cells by Myc and the p19ARF-p53 pathway. J. Cell Biol. 183, 1243–1257.

Nicklas, S., Otto, A., Wu, X., Miller, P., Stelzer, S., Wen, Y., Kuang, S., Wrogemann, K., Patel, K., Ding, H., Schwamborn, J.C., 2012. TRIM32 regulates skeletal muscle stem cell differentiation and is necessary for normal adult muscle regeneration. PLoS ONE 7, e30445.

Nuber, S., Petrasch-Parwez, E., Winner, B., Winkler, J., Von Hörsten, S., Schmidt, T., Boy, J., Kuhn, M., Nguyen, H.P., Teismann, P., Schulz, J.B., Neumann, M.,

Pichler, B.J., Reischl, G., Holzmann, C., Schmitt, I., Bornemann, A., Kuhn, W., Zimmermann, F., Servadio, A., Riess, O., 2008. Neurodegeneration and motor dysfunction in a conditional model of Parkinson's disease. J. Neurosci. 28, 2471–2484.

Patthey, C., Edlund, T., Gunhaga, L., 2009. Wnt-regulated temporal control of BMP exposure directs the choice between neural plate border and epidermal fate. Development 136, 73–83.

Reymond, A., Meroni, G., Fantozzi, A., Merla, G., Cairo, S., Luzi, L., Riganelli, D., Zanaria, E., Messali, S., Cainarca, S., Guffanti, A., Minucci, S., Pelicci, P.G., Ballabio, A., 2001. The tripartite motif family identifies cell compartments. EMBO J. 20, 2140–2151.

Rybak, A., Fuchs, H., Smirnova, L., Brandt, C., Pohl, E.E., Nitsch, R., Wulczyn, F.G., 2008. A feedback loop comprising lin-28 and let-7 controls pre-let-7 maturation during neural stem-cell commitment. Nature Cell Biology 10, 987–993.

Sánchez-Danés, A., Richaud-Patin, Y., Carballo-Carbajal, I., Jiménez-Delgado, S., Caig, C., Mora, S., Di Guglielmo, C., Ezquerra, M., Patel, B., Giralt, A., Canals, J.M., Memo, M., Alberch, J., López-Barneo, J., Vila, M., Cuervo, A.M., Tolosa, E., Consiglio, A., Raya, A., 2012. Disease-specific phenotypes in dopamine neurons from human iPS-based models of genetic and sporadic Parkinson's disease. EMBO Mol Med 4, 380–395.

Santpere, G., Ferrer, I., 2009. LRRK2 and neurodegeneration. Acta Neuropathol. 117, 227–246.

Schapira, A.H., 1999. Mitochondria in the aetiology and pathogenesis of Parkinson's disease. Parkinsonism Relat. Disord. 5, 139–143.

Schwamborn, J.C., Berezikov, E., Knoblich, J.A., 2009. The TRIM-NHL Protein TRIM32 Activates MicroRNAs and Prevents Self-Renewal in Mouse Neural Progenitors. Cell 136, 913–925.

Shimura, H., Schlossmacher, M.G., Hattori, N., Frosch, M.P., Trockenbacher, A., Schneider, R., Mizuno, Y., Kosik, K.S., Selkoe, D.J., 2001. Ubiquitination of a new form of alpha-synuclein by parkin from human brain: implications for Parkinson's disease. Science 293, 263–269.

Shin, N., Jeong, H., Kwon, J., Heo, H.Y., Kwon, J.J., Yun, H.J., Kim, C.-H., Han, B.S., Tong, Y., Shen, J., Hatano, T., Hattori, N., Kim, K.-S., Chang, S., Seol, W., 2008. LRRK2 regulates synaptic vesicle endocytosis. Exp. Cell Res. 314, 2055–2065.

Shmelkov, S.V., St.Clair, R., Lyden, D., Rafii, S., 2005. AC133/CD133/Prominin-1. The International Journal of Biochemistry & Cell Biology 37, 715–719.

Smith, W.W., Pei, Z., Jiang, H., Dawson, V.L., Dawson, T.M., Ross, C.A., 2006. Kinase activity of mutant LRRK2 mediates neuronal toxicity. Nat. Neurosci. 9, 1231–1233.

Tong, Y., Yamaguchi, H., Giaime, E., Boyle, S., Kopan, R., Kelleher, R.J., 3rd, Shen, J., 2010. Loss of leucine-rich repeat kinase 2 causes impairment of protein degradation pathways, accumulation of alpha-synuclein, and apoptotic cell death in aged mice. Proc. Natl. Acad. Sci. U.S.A. 107, 9879–9884.

Van den Berge, S.A., Van Strien, M.E., Korecka, J.A., Dijkstra, A.A., Sluijs, J.A., Kooijman, L., Eggers, R., De Filippis, L., Vescovi, A.L., Verhaagen, J., Van de Berg, W.D.J., Hol, E.M., 2011. The proliferative capacity of the subventricular zone is maintained in the parkinsonian brain. Brain 134, 3249–3263.

Wallace, D.C., Fan, W., Procaccio, V., 2010. Mitochondrial energetics and therapeutics. Annu Rev Pathol 5, 297–348.

West, A.B., Moore, D.J., Biskup, S., Bugayenko, A., Smith, W.W., Ross, C.A., Dawson, V.L., Dawson, T.M., 2005. Parkinson's disease-associated mutations in leucine-rich repeat kinase 2 augment kinase activity. Proc. Natl. Acad. Sci. U.S.A. 102, 16842–16847.

Winner, B., Melrose, H.L., Zhao, C., Hinkle, K.M., Yue, M., Kent, C., Braithwaite, A.T., Ogholikhan, S., Aigner, R., Winkler, J., Farrer, M.J., Gage, F.H., 2011. Adult neurogenesis and neurite outgrowth are impaired in LRRK2 G2019S mice. Neurobiol. Dis. 41, 706–716.

Winner, B., Rockenstein, E., Lie, D.C., Aigner, R., Mante, M., Bogdahn, U., Couillard-Despres, S., Masliah, E., Winkler, J., 2008. Mutant alpha-synuclein exacerbates age-related decrease of neurogenesis. Neurobiol. Aging 29, 913–925.

Wulczyn, F.G., Smirnova, L., Rybak, A., Brandt, C., Kwidzinski, E., Ninnemann, O., Strehle, M., Seiler, A., Schumacher, S., Nitsch, R., 2007. Post-transcriptional regulation of the let-7 microRNA during neural cell specification. FASEB J 21, 415–426.

Zhang, S.C., Wernig, M., Duncan, I.D., Brüstle, O., Thomson, J.A., 2001. In vitro differentiation of transplantable neural precursors from human embryonic stem cells. Nat. Biotechnol. 19, 1129–1133.

Zhao, C., Deng, W., Gage, F.H., 2008. Mechanisms and Functional Implications of Adult Neurogenesis. Cell 132, 645–660.

7 Appendix

7.1 Abbreviations

α	1. anti
	2. alpha
µM	micromolar
AA	ascorbic acid
BCA	bicinchoninic acid
BDNF	brain-derived neurotrophic factor
BSA	bovine serum albumin
° C	degree Celsius
CD133	prominin 1
cDNA	complementary DNA
cm	centimeter
CNS	central nervous system
CO₂	carbon dioxide
CTRL	control
d	day
DAPI	4', 6-Diamidino-2-phenylindol
dbcAMP	Dibutyryladenosine cyclic monophosphate
DMEM	modified Dulbecco's modified Eagle's medium
DMSO	dimethylsulfoxid
DNA	deoxyribonucleic acid
DTT	dithiothreitol
E	embryonic day
EGFP	enhanced green fluorescent protein
ESCs	embryonic stem cells
et. al.	et alteri /-a /-um (and others)
FGF 8	fibroblast growth factor 8
FGF2	fibroblast growth factor 2
for	forward

GDNF	Glial cell-derived neurotrophic factor
GFP	green fluorescent protein
h	hour
HEK293T	human embryonic kidney cells 293 T
hmNPCs	human mesencephalic neural progenitor cells
IP	immunoprecipitation
kDa	kilo Dalton
l	liter
M	molar
mA	milliampere
µg	microgram
µl	microliter
miRNA	micro RNA
mg	milligram
min	minute
ml	milliliter
mm	millimeter
mRNA	messenger RNA
miRNA	micro RNA
NE cells	neuroepithelial stem cells
ng	nanogram
nm	nanometer
NSCs	neural stem cells
p	1. passage 2. p-Value
PAGE	polyacrylamide gel electrophoresis
PBS	phosphate buffered saline
PCR	polymerase chain reaction
PD	Parkinson's disease
PFA	paraformaldehyde
pH	potentium hydrogenii (lat.)
PMA	purmorphamin

PNS	peripheral nervous system
rev	reverse
RMS	rostral migratory stream
ROS	reactive oxygen species
rpm	rounds per minute
RT	1. room temperature 2. reverse transcription
s	second
s.e.m	standard error of the mean
SA-β-galactosidase	senescence-associated β-galactosidase
SDS	sodium dodecyl sulphate
SGZ	subgranular zone
SVZ	subventricular zone
TEMED	N,N,N',N'- Tetramethylethyldiamine
TGF-β	transforming growth factor β
UTR	untranslated region
V	Volt
WT	wildtype
ZO1	zonula occludens 1

7.2 List of Figures

7.3 List of Tables

Acknowledgement

First I want to thank Jens Schwamborn for the great opportunity to do my master thesis in his lab. He challenged and guided me through this time and gave me a lot of self-confidence.

Thanks to Peter Reinhardt for the supply with the neuroepithelial cells.

Furthermore, I would like to thank all the group members for the great support and the advices. Special thanks to my colleges Kathrin, Thomas and Sarah who shared the office with me. It was always entertaining and the out-of-the lab activities helped me to keep my mind free and creative. I am glad that we became such good friends and you made the time a lot easier for me.

Dank gebührt ebenfalls meinen Eltern, die mir diesen Lebensweg ermöglichen und mir stets mit Rat und Tat zur Seite stehen. Ich danke auch meinen Geschwistern für die aufmunternden Worte in schwierigen Zeiten und die Geduld in manchen Lebenslagen.

Zuletzt danke ich meinem Freund Stefan, dank dir habe ich überhaupt den Schritt gewagt und die Chance ergriffen, diese großartige Erfahrung zu machen. Vielen Dank für deine Unterstützung und deine aufbauenden Worte

Curriculum Vitae

Name   Ingeborg Menzl

Nationality   Austria

Tertiary education

01/2012 – 09/2012 Master thesis, Research group Stem cell biology and Regeneration, Institute of Cell Biology, University of Münster, Germany

Thesis: *Ageing of neural stem cells in a Parkinson's disease Model*

Since 2010 Master in Molecular Biology at the University of Vienna

2007 - 2010 Bachelor Molecular Biology at the University of Salzburg and Johannes Kepler University of Linz

School education

2002 – 2007   Business School of Steyr
              Subject: Informatics

1998 - 2002   Secondary School Haidershofen

1995-1998   Elementary School Haidershofen

Practical training

08 – 09/2009 Practical training at the Donau University Krems, Cell Biology

08 – 09/2011 Baxter AG, QC Microbiology Laboratory

10 – 11/2011 Practical training at the MPFL Vienna in the Laboratory of
              Prof. Rotheneder; Cell Signalling

Languages

German (native)

English (fluent)

Spanish (basics)

Conferences

2012   Conference of the Kompetenznetzwerks Stammzellforschung NRW, Herne

2012   Molecular Cell Dynamics (SFB629) Conference, Topic: Cell Polarity, Münster

Publications

Bahnassawy L., Palm T., Menzl I., Quandel T., Birzele F., Gillardon F.,Schwamborn J.C. (2012). The Parkinson's disease associated LRRK2 mutation R1441G inhibits neuronal differentiation of neural stem cells (in Revision)